Design of a Low-profile Wideband Circularly Polarized Antenna and its Array at Ka-band

Luoqing Wang

Department of Electrical & Computer Engineering

McGill University, Montreal

August, 2021

A thesis submitted to McGill University in partial fulfillment of the requirements of the degree of

Master of Science

Abstract

In this thesis, a low-profile wideband circularly polarized magnetoelectric (ME) dipole antenna with parasitic patches is proposed. The proposed element, consisting of a pair of rotationally symmetric inverted L-shape patches acting as an electric dipole with four parasitic patches, is fed by a longitudinal slot etched on top of a short-end substrate integrated waveguide (SIW), with a height of only $0.07\lambda_0$, where λ_0 equals the free space wavelength at 28GHz. The simulation shows that the element achieves a wide impedance and 3dB axial ratio (AR) bandwidth of 22.1% (from 24.64 to 30.77GHz) and 20.1% (from 25.22 to 30.85GHz) respectively, and a gain of 8.0 ± 0.7 dBic over the operating band. To verify the performance of the antenna element, an antenna prototype that combines the antenna element with additional transmission lines and walls aiming to suppress the surface wave and provide better isolation from surroundings has been designed, fabricated, and measured. Due to the above modifications, the prototype reveals different results compared to the element; the measured results indicate that the fabricated antenna prototype can achieve an impedance and 3dB-AR bandwidth of 19.7% (from 24.96 to 30.4GHz) and 17.5% (from 25.67 to 30.59GHz) respectively, and a gain of 7.2 ± 1.1 dBic over the operating band. Finally, based on the proposed antenna element, a four-element linear circularly polarized antenna array with a SIW feeding network has been designed, fabricated, and measured. The array has a wide measured impedance and 3dB-AR bandwidth of 17.39% (from 25.42 to 30.26GHz) and 16.93% (from 25.57 to 30.30GHz) respectively, and a peak gain of 12.9dBic without using the sequential feed.

Abrégé

Dans cette thèse, une antenne dipôle magnétoélectrique (ME) à large bande et à large bande avec des plaques parasitaires est proposée. L'élément proposé, constitué d'une paire de patchs en forme de L inversé symétriques en rotation agissant comme un dipôle électrique avec quatre plaques parasitaires, est alimenté par une fente longitudinale gravée au-dessus d'un guide d'ondes intégré à substrat court (SIW), avec une hauteur de seulement 0,07 λ_0, où λ_0 est égal à la longueur d'onde de l'espace libre à 28 GHz. La simulation montre que l'élément atteint une large impédance et une bande passante de rapport axial (AR) de 3 dB de 22,1 % (de 24,64 à 30,77 GHz) et 20,1 % (de 25,22 à 30,85 GHz) respectivement, et un gain de 8,0 ± 0,7 dBic sur la bande d'exploitation. Pour vérifier les performances de l'élément d'antenne, un prototype d'antenne qui combine l'élément d'antenne avec des lignes de transmission et des murs supplémentaires visant à supprimer l'onde de surface et à fournir une meilleure isolation de l'environnement a été conçu, fabriqué et mesuré. En raison des modifications ci-dessus, le prototype révèle des résultats différents par rapport à l'élément ; les résultats mesurés indiquent que le prototype d'antenne fabriqué peut atteindre une impédance et une bande passante 3dB-AR de 19,7% (de 24,96 à 30,4 GHz) et 17,5% (de 25,67 à 30,59 GHz) respectivement, et un gain de 7,2 ± 1,1 dBic sur la bande d'exploitation. Enfin, sur la base de l'élément d'antenne proposé, un réseau d'antennes linéaires à polarisation circulaire à quatre éléments avec un réseau d'alimentation SIW a été conçu, fabriqué et mesuré. La matrice a une large impédance mesurée et une bande passante 3dB-AR de 17,39 % (de 25,42 à 30,26 GHz) et 16,93 % (de 25,57 à 30,30 GHz) respectivement, et un gain de crête de 12,9 dBic sans utiliser l'alimentation séquentielle.

Acknowledgements

I would like express my sincere gratitude to my supervisor Prof. Zeljko Zilic for his guidance and encouragement throughout the course of this thesis.

I would like to thank Mr. Hongquan Fu and Mr. Jianshu Shi for fabricating and measuring the proposed antennas.

I also would like to acknowledge CMC Microsystems for the provision of Ansys HFSS that facilitated this research.

Table of Contents

List of Abbreviations

5G fifth generation mobile network

AR axial ratio

AUT antenna under test

BW bandwidth

CP circular polarization

EM electromagnetic

FR2 frequency range 2

IoT internet of things

LHCP left-hand circular polarization

LP linear polarization

ME magnetoelectric

mmWave millimeter wave

PCB printed circuit board

RHCP right-hand circular polarization

SIW substrate integrated waveguide

SLL sidelobe level

SRT sequential rotated technique

TE transverse electric

TM transverse magnetic

List of Figures

List of Tables

Chapter 1

Introduction

1.1 Motivation

With the rapid growth of internet-of-things(IoT) and fifth-generation mobile networks(5G), antennas that are crucial to a wireless communication system's performance have started gaining more attention, especially those operating in millimeter band. Currently, there is no strict boundary of the millimeter band. Some papers [6] state the range of millimeter band as 30GHz to 300GHz, but some works [19] indicate the range starting at 24.25GHz or 26.5GHz (Ka-Band), which are aligned with frequency range 2 (FR2) of 5G communication systems. This thesis follows the latter definition to describe the millimeter band.

With a shorter wavelength, millimeter-wave (mmWave) antennas have several advantages over those operating in lower frequencies. First, mmWave antennas have a smaller physical dimension and could be easily integrated into smaller devices. Second, as mmWave antennas operating at a higher operating frequency, they could transmit data at a faster rate and meet the increasing demand of data flow. Moreover, in contrast to lower frequency bands, in which most of the spectrum resources have already been occupied by existing applications, the millimeter band still has plenty of resources available for novel designs and products. Finally, the millimeter-wave antenna could provide higher resolution comparing to ones in lower frequencies, which allows the development of applications with high precision requirements such as object detection [31] and body vital signs monitoring [52].

However, with higher frequency and shorter wavelength, there are also various challenges when designing a mmWave antenna, such as high free-space path loss and transmission line loss. Free-space path loss describes the loss in signal strength during signal transmission between transmitter and receiver in free space and increases with the operating frequency of an antenna [34]. A way to reduce the free-space path loss is to improve the overall gain of the antenna by placing multiple identical antenna elements into an antenna array at an optimal distance to form a single high gain narrow beam [38].

Transmission line loss is another major challenge for a mmWave antenna. At lower frequencies, antennas utilize a feeding network consisting of microstrip lines or coaxial cables. However, at mmWave frequency, the transmission loss using traditional methods becomes significant and negatively impacts the antenna performance, especially for an antenna array. A way to solve it is to use a waveguide. However, the conventional waveguide is expensive to produce and complicated to integrate with planar circuits due to its larger size. The substrate integrated waveguide [22] was proposed to overcome this issue: it could be easily fabricated at a lower cost on a PCB board and has fewer space constraints comparing to conventional rectangular waveguides while maintaining low transmission loss.

Among different antennas, various types of circularly polarized (CP) antennas, such as microstrip patch [51] [16] [40] and cavity [32] [4] [17] antennas, have received more attention due to their ability to suppress the multipath loss and polarization mismatch loss [21]. However, most of those works have a limited 3dB axial ratio (AR) bandwidth. A way to address this issue is to introduce the concept of the magnetoelectric (ME) dipole [28].

The ME dipole antenna was proposed by [29]. By exciting a planar electric dipole and a shorted patch antenna acting as a magnetic dipole simultaneously, the ME dipole antenna could achieve excellent electrical performance such as wide impedance bandwidth, low back radiation, and symmetrical radiation patterns in both E and H-plane. Various circularly polarized ME dipole antennas have been introduced in the past [26] [28]. However, most of those works still follow the conventional guideline proposed in [29] and utilize substrates with a height of a quarter wavelength which complicate the integration process with front-end circuits. A low-profile wideband CP ME dipole antenna is highly desired.

1.2 Contribution

The contributions of this thesis are organized as follows:

1. Chapter 2 provides background information of basic antenna parameters, substrate integrated waveguide (SIW), magnetoelectric(ME) dipole antennas, and antenna arrays.

2. In Chapter 3, a novel low-profile wideband circularly polarized magnetoelectric dipole antenna with parasitic patches is proposed. The proposed element is fed by a longitudinal slot etched on top of a short-end substrate integrated waveguide (SIW) and has achieved a wide overlapped bandwidth of 19.8%(25.22GHz to 30.77GHz) and reduced the thickness of conventional ME dipole antenna from 0.25 to 0.1 λ_s , where $\lambda_s = \lambda_0 / \sqrt{\epsilon_r}$ (λ_0 and ϵ_r represent the free space wavlength at 28GHz and relative permittivity of the substrate material respectively). To verify the proposed element, an antenna prototype that combines the antenna element with additional transmission lines and walls is designed and fabricated. Due to the above modifications, the prototype reveals different results compared to the original antenna element; the antenna prototype achieves a wide measured impedance and 3dB-AR bandwidth of 19.7%(24.96 to 30.4GHz) and 17.5%(25.67 to 30.59GHz) respectively, and a gain of 7.2 $\pm$ 1.1 dBic over the operating band.

3. In Chapter 4, I first determine the optimal distance between antenna elements. Then, a 1x4 SIW power divider that distributes input energy uniformly to four output ports with the same phase is designed. Finally, a four-element linear CP antenna array with the SIW feeding network is designed and fabricated based on the proposed power divider and antenna elements. The antenna array achieves a wide measured impedance and 3dB-AR bandwidth of 17.39%(from 25.42 to 30.26GHz) and 16.93%(from 25.57 to 30.30GHz) respectively, and a peak gain of 12.9dBic without using the sequential feed.

4. A research paper entitled *Design of a Ka-Band Low-Profile Wideband Circularly Polarized Magneto-Electric Dipole Antenna With Parasitic Patches and Its Array* has been produced by *Luoqing Wang and Zeljko Zilic* and submitted on July 28, 2021 to the Asia-Pacific Microwave Conference taking place in Brisbane, Australia in November, 2021.

Chapter 2

Background

2.1 Antenna Basics

2.1.1 Return loss

The return loss is related to the reflection coefficient Γ or S_{11}; it determines the extent to which the power has been reflected from the antenna to the transmission line [39], pg.112. The return loss is measured on a logarithmic scale, as seen in the Equation 2.1. Ideally, all energy from the transmission line should be transferred to the antenna for radiation. However, this is hard to achieve due to the impedance mismatch between the transmission line and the antenna. As a result, in this thesis, the impedance bandwidth is defined as the range of frequencies which has the return loss or $|S_{11}|$ less than -10dB. To better compare with other works, the fractional bandwidth [39], pg.218, has been used, which is defined as seen in the Equation 2.2 where f_u and f_l represent the upper and lower frequency of the operating band respectively.

$$Return\ Loss = -20log_{10}|\Gamma| \tag{2.1}$$

$$Fractional\ Bandwidth = 2\frac{f_u - f_l}{f_u + f_l} \tag{2.2}$$

2.1.2 Radiation Pattern

The antenna radiation pattern is a graphic representation of the field or power radiated by the antenna to the free space in the far-field region [5], pg.25-30. The radiation pattern could be three-dimensional, or one can observe two-dimensional principal planes of the 3D pattern, depending on the usage. In this thesis, the radiation pattern refers to the power pattern, which represents the power density at a constant radius from the antenna on a logarithmic scale. A commonly used spherical coordinate system from [5], pg.26 is adopted for antenna analysis as shown in the Figure 2.1. For directional antennas, the main lobe, the radiation lobe with maximum radiation, should point to the desired direction. In contrast, the minor lobes, the radiation lobes other than the main lobe, should be minimized to avoid the possible interference [5], pg.25-30.

2.1.3 Directivity and Gain

The directivity of an antenna is defined by the following Equation 2.3 from [5], pg. 41, where D, U, U_0, and P_{rad} represent directivity, radiation intensity, radiation intensity of isotropic source, and total radiated power respectively. In other words, the directivity is a ratio of the radiation intensity of an antenna in a specific direction to the radiation

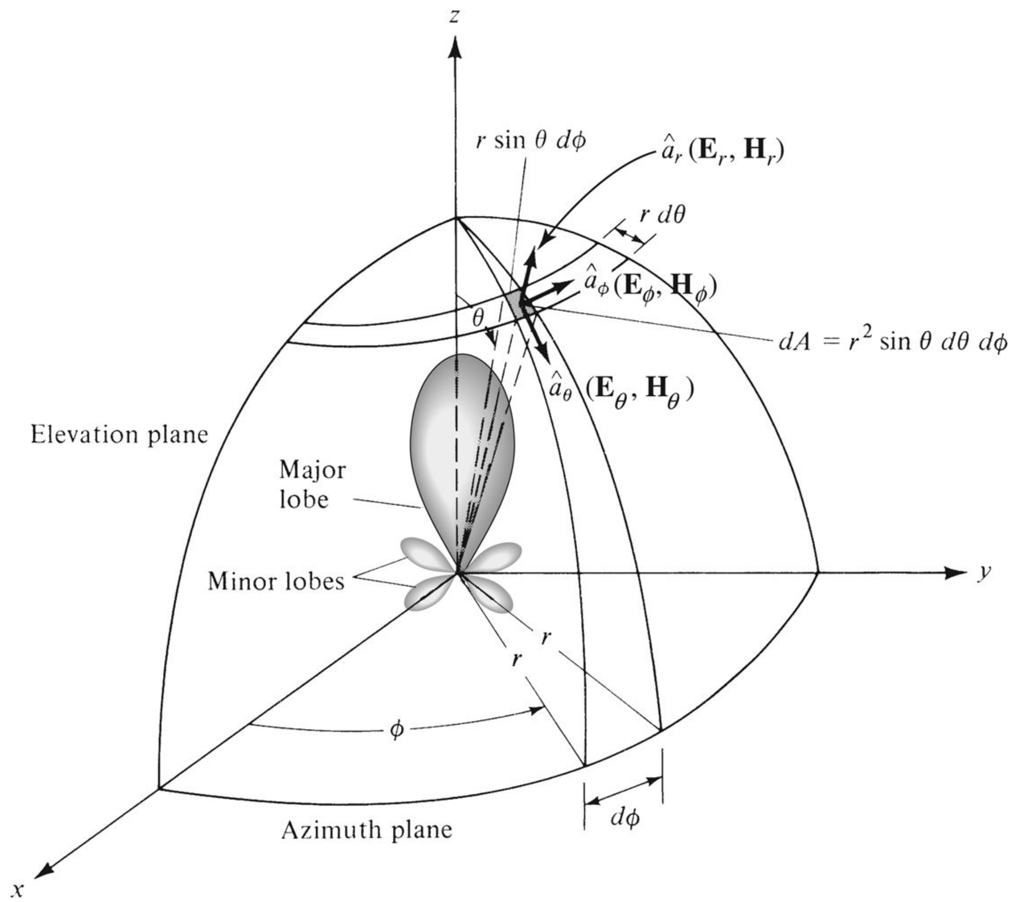

Figure 2.1: Coordinate system for antenna analysis, adopted from [5], pg.26

intensity of an isotropic source, an ideal imaginary antenna that radiates power equally to all directions. If the direction is not given, the direction of the maximum radiation intensity is assumed as seen in the Equation 2.4 from [5], pg.41.

$$D = \frac{U}{U_0} = \frac{4\pi U}{P_{rad}} \tag{2.3}$$

$$D_{max} = \frac{U_{max}}{U_0} = \frac{4\pi U_{max}}{P_{rad}} \tag{2.4}$$

Gain is another important aspect of an antenna that determines to what extent the power is radiated in each direction compared to an isotropic source. It is similar to the directivity introduced above but taking the efficiency of the antenna into consideration as shown in the Equation 2.5 from [5], pg. 61-63, where e_{cd} represents the antenna radiation efficiency which takes conduction and dielectric losses of the antenna structure into the consideration.

$$Gain = e_{cd}D \tag{2.5}$$

2.1.4 Polarization

Polarization is an essential characteristic of an antenna; it is the same as the polarization of the wave radiated by the antenna and defined as the pattern traced out by the tip of the electric field vector as a function of time at a fixed point [5], pg.66-69. Two antennas need to match the polarization of each other to reach maximum efficiency. There are three types of polarization: linear, circular, and elliptical, as shown in the Figure 2.2. A Linear polarized antenna has the electric field vector, which is always oriented along the same axis at a fixed point. An antenna is circularly polarized if the tip of the electric field vector traces a circle at a fixed point in space. Based on the rotation of the electric field vector, CP antennas could be further categorized into two types: left-hand circularly polarized(LHCP) antennas if the vector rotates counterclockwise and right-hand circularly polarized(RHCP) antennas if the vector rotates clockwise. An antenna is elliptically polarized if the tip of the electric field vector traces an ellipse at a fixed point in space.

The polarization ellipse from [5], pg.67, is shown in the Figure 2.3, where OA, OB, E_{y0}, and E_{x0}, τ represents the major axis, minor axis, y-component of the electric field, x-component of the electric field, tilt of the ellipse relative to y-axis respectively. Under a perfect condition, a circularly polarized antenna should have the axial ratio (AR), a ratio of the major and minor axis of the polarization ellipse, of 1 or 0dB [5], pg.66-69. In this thesis, the axial ratio (AR) bandwidth is defined as the range of frequencies that has an axial ratio less than 3dB. Moreover, CP antennas still need to have acceptable return loss to work properly. Therefore, the overlapped bandwidth has also been used and is defined as the range of frequencies which has $|S_{11}|$ less than -10dB and an axial ratio less than 3dB.

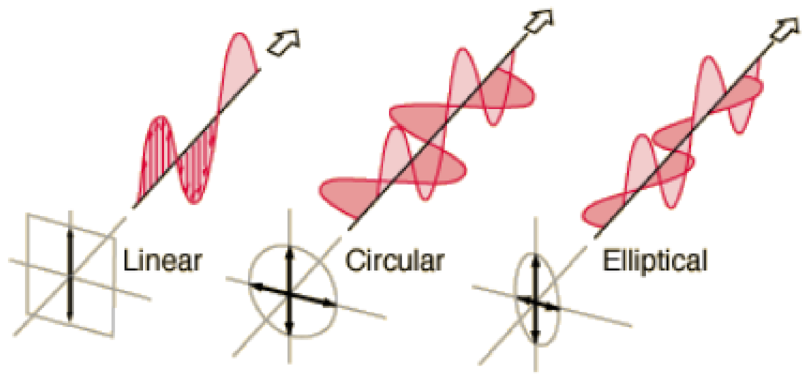

Figure 2.2: Types of polarization, adopted from [36]

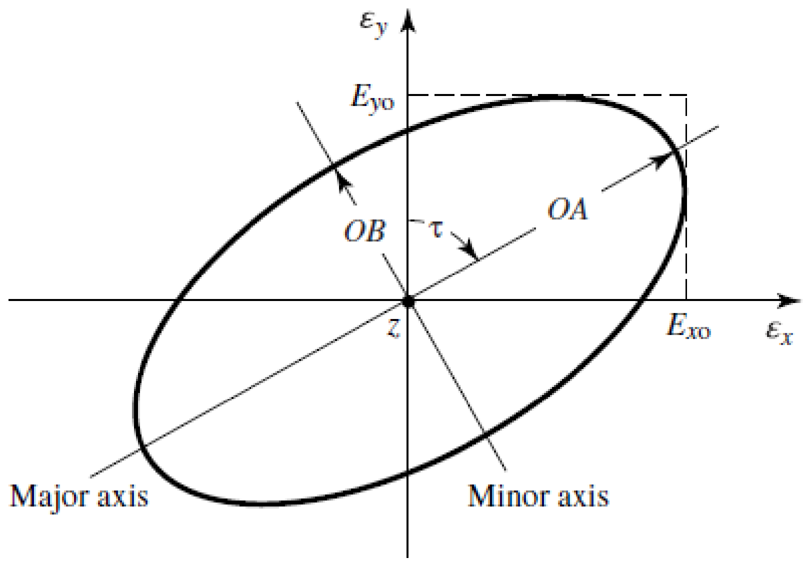

Figure 2.3: Polarization ellipse, adopted from [5], pg. 67

2.2 Substrate Integrated Waveguide

In the millimeter-wave band, the transmission loss has become a non-negligible problem for traditional transmission lines such as microstrip lines and suspended lines. A waveguide is a special form of transmission line containing EM waves inside a hollow or dielectric-filled metal tube and transports them from one point to another as shown in the Figure 2.4 from [9]. Comparing to other transmission methods, waveguides have several advantages such as less transmission loss, higher isolation, and lower leakage [18] which makes it an ideal candidate for transporting millimeter waves. A waveguide could be further categorized into different types based on the cross-section shape, such as rectangular and circular waveguides. The waveguide also supports waves in both TE(transverse electric) and TM(transverse magnetic) mode; TE mode indicates that the electric field is perpendicular to the direction of propagation, while TM mode represents the magnetic field is perpendicular to the direction of propagation. However, as the conventional waveguide at mmWave frequencies requires a high-cost precision machining process and has a larger physical dimension, it is expensive to manufacture and complicated to integrate with the planar circuit [10].

To overcome those issues, substrate integrated waveguide (SIW), a special rectangular dielectric-filled waveguide in a planar form, has been proposed [18]; it has well-preserved advantages of a conventional waveguide such as low transmission loss while maintaining a much lower profile. The SIW is embedded inside a metal-clad substrate with two rows of metallic vias in between, as shown in the Figure 2.5. Even though the SIW has similar properties as a regular waveguide, there are still some differences. The SIW has leakage

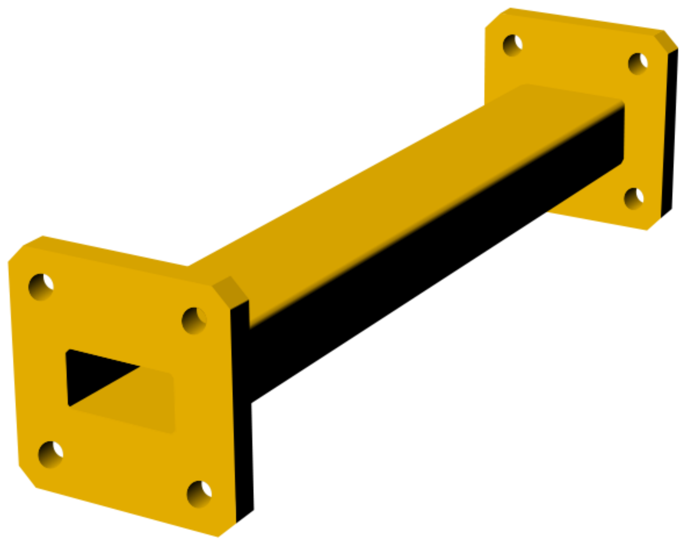

Figure 2.4: 3D view of a rectangular waveguide, adopted from [9]

loss due to the gaps between the vias [46]; the energy could escape from the gaps, and the leakage loss increases with spacing. Moreover, as those gaps prevent longitudinal current from traveling, the SIW only supports waves that excite in the TE mode [46]. Furthermore, due to the periodic structure, the SIW might experience the bandgap effect [11]; it is important to ensure that there are no bandgaps within the operating bandwidth when designing a SIW.

Different transition schemes have been used to connect to SIW, such as waveguide-to-SIW [25], coplanar waveguide-to-SIW [41], and microstrip line-to-SIW [23]. However, most existing works only provide rough guidelines or structures for the transition component; there is a limited number of studies that offer mathematical procedures for calculating the dimensions and often require a time-consuming parameter search. Due to the time and manufacturing limitations, we utilize the 50-ohm microstrip line, which could match the impedance of a standard connector and provide better overall efficiency, to feed the SIW directly in this thesis.

2.2.1 Design of a SIW waveguide

In this thesis, the design process from [11] [46] have been studied and used as guidelines. The process contains the following steps:

1. Choose substrate material and select $s/d(<2.0)$ and $d/w(<1/5)$ where s is the distance between the center of vias, d is the diameter of the vias, and w is the width of the SIW.

2. Calculate equivalent waveguide width using the Equation 2.1 where λ_c is the wavelength of the cut-off frequency and ε_r is the relative permittivity of the substrate material.

$$w_{eff} = \frac{c}{2f_c\sqrt{\varepsilon_r}} \tag{2.6}$$

3. Calculate w by solving the Equation 2.2

$$w_{eff} = w - 1.08 \cdot \frac{d^2}{s} + 0.1 \cdot \frac{d^2}{w} \tag{2.7}$$

4. Calculate d and s. For this step, the size of d and s is mainly determined by the availability of drills from the manufacture.

Following the above steps, we have calculated the SIW network's dimension based on our target characteristics, which should have a working frequency band between 24GHz to 32GHz. The substrate material in our design is Rogers 5880 with a height of 0.787mm, a dielectric loss tangent of 0.0009, a relative permittivity of 2.2. The dimension of the SIW could be found in the Table 2.1.

Table 2.1: Dimension of the SIW prototype

Parameter	w	d	s	L
Value	5.85mm	0.7mm	1.3mm	30cm

To verify the design choice, a SIW with two wave ports on each end and a length of 30cm is simulated using HFSS as shown in the Figure 2.5. The result shown in the Figure 2.6 indicates that the selected parameters of the SIW meet the requirement by providing a stable operating frequency band between 24GHz to 32GHz which covers our targeted working frequency; the return loss(S_{11}) is less than -15dB, and the insertion loss(S_{21}) is around 0.2dB for the frequency range from 24GHz to 32GHz over a 30cm distance.

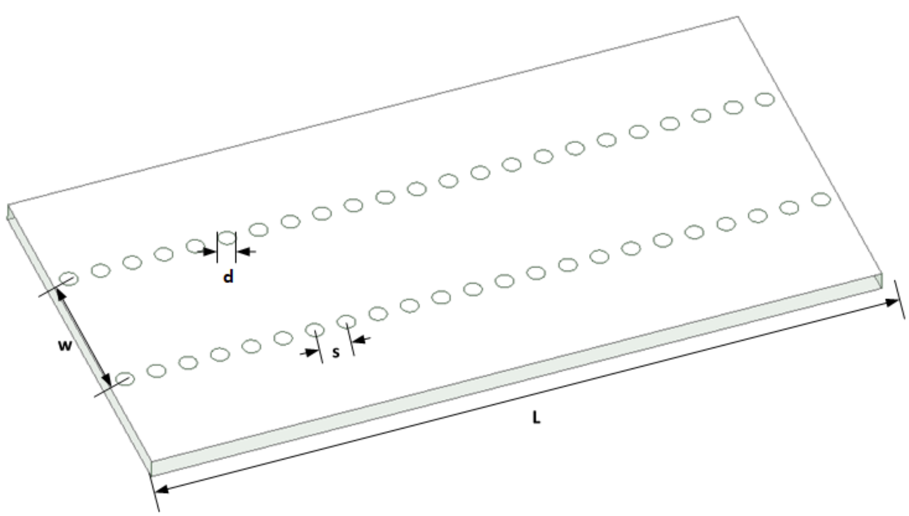

Figure 2.5: Geometry of the SIW prototype

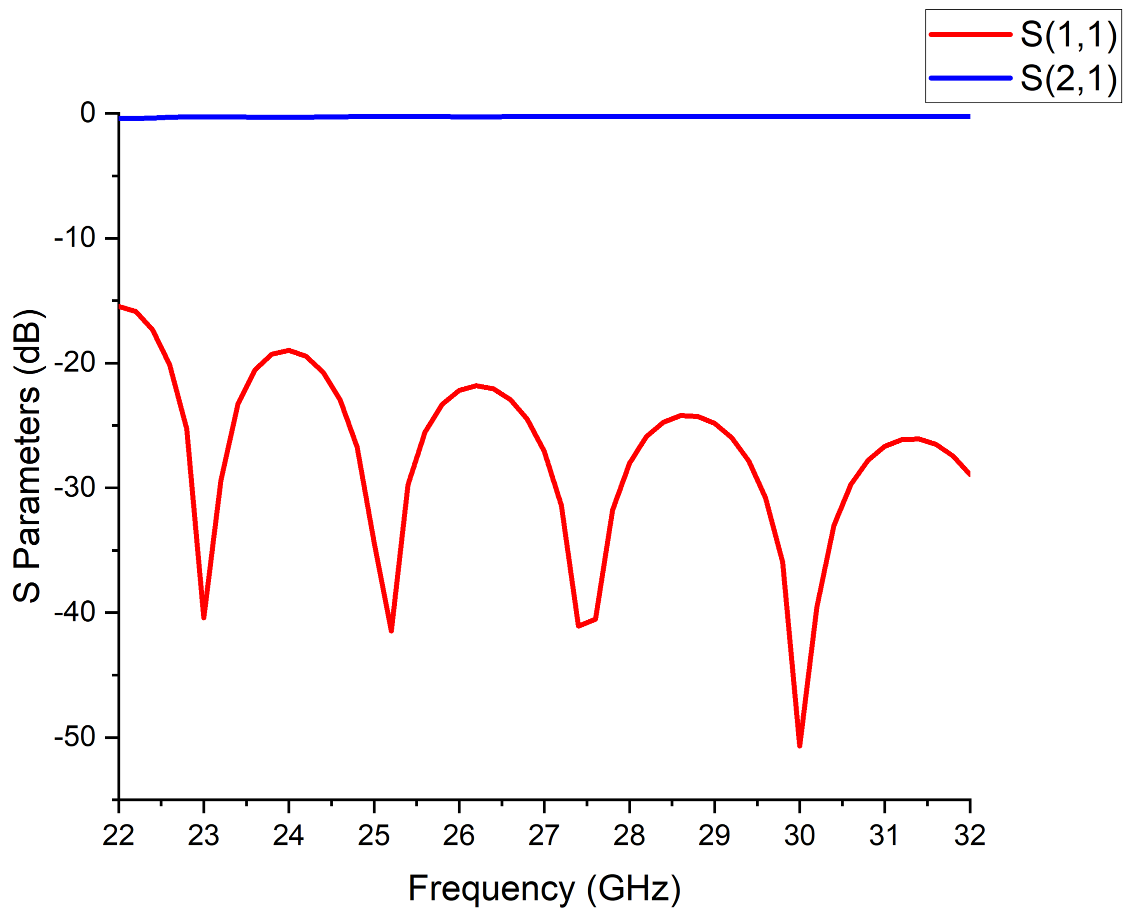

Figure 2.6: Simulated S-parameters of the SIW prototype

2.3 Magnetic Electric Dipole Antenna

The concept of a complementary antenna consisting of an electric dipole and a magnetic dipole was proposed by Clavin in 1954 [8]. The original design consists of two complementary antennas: a half-wavelength electric dipole and an open-end coaxial line carrying TE_{11} mode acting as a magnetic dipole. An electric dipole has a figure-8 and a figure-O shape in the E and H plane, respectively, while the magnetic dipole has a figure-O and figure-8 shape as seen in the Figure 2.7. By feeding both antennas with proper amplitude and phase simultaneously, a unidirectional(cardioid) pattern with low back radiation can be realized.

Magnetoelectric (ME) dipole antenna is a type of complementary antenna introduced by Luk and Huang in 2006 [29]. The ME dipole antenna has a similar concept as the original complementary antenna proposed in [8], which combines a planar electric dipole and a magnetic dipole realized by a shorted patch antenna as shown in the Figure 2.8. By exciting the electric and magnetic dipoles with proper amplitude and phase simultaneously, the ME dipole antenna could achieve excellent electrical performance such as wide impedance bandwidth, low back radiation, and symmetrical radiation patterns in E and H-plane.

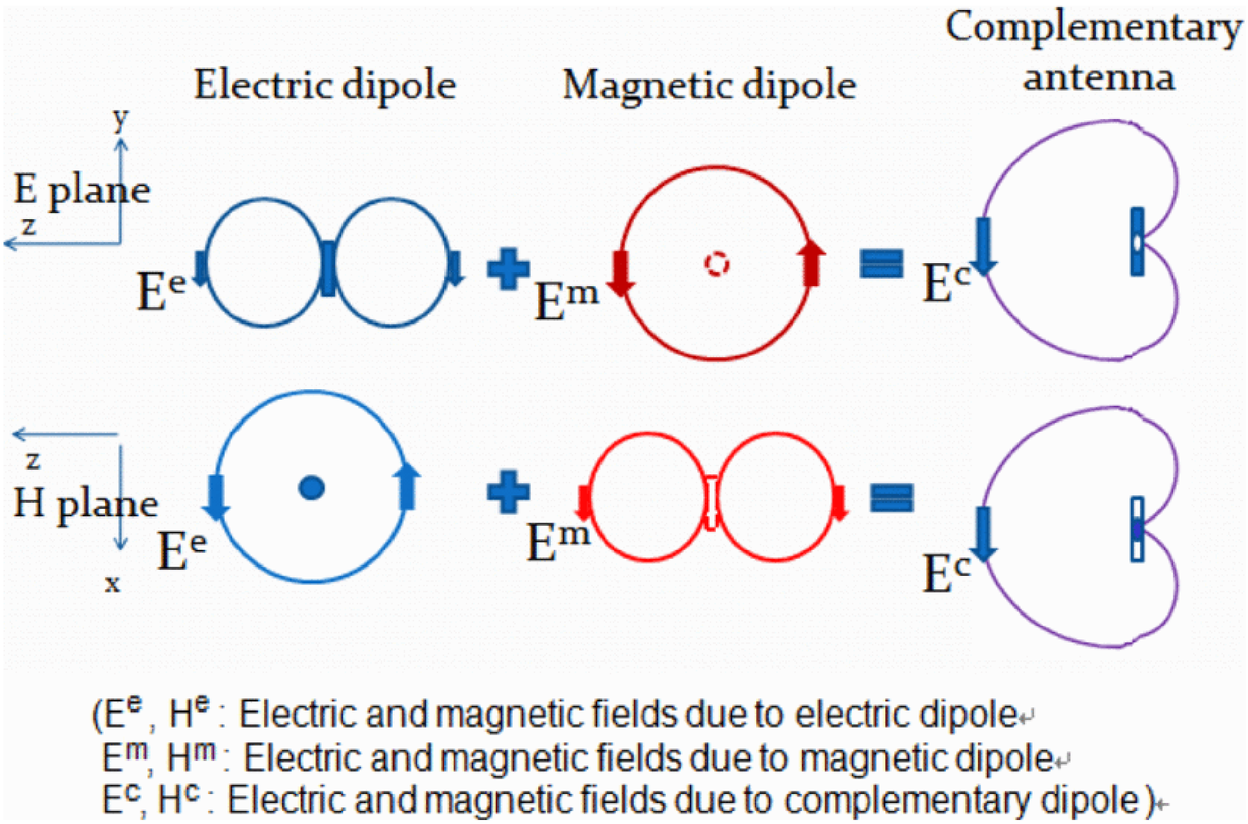

Figure 2.7: Complementary antenna concept, adopted from [30]

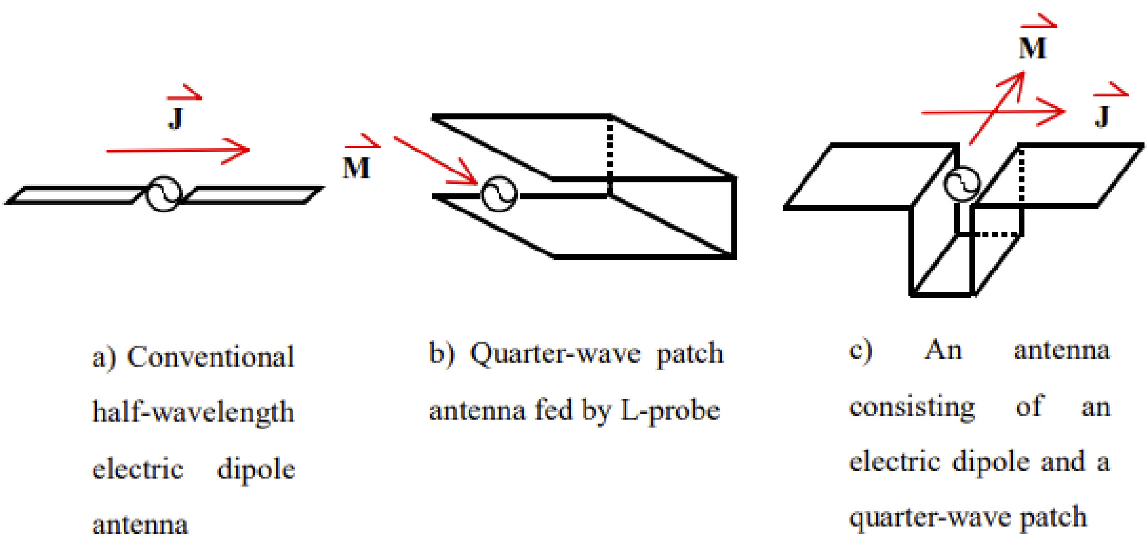

Figure 2.8: Structure of the ME dipole antenna, adopted from [29]

2.3.1 Circularly Polarized Magnetoelectric Dipole Antenna

In this thesis, circular polarization is of principal interest, due to its ability to suppress multipath interferences and reduce the loss of polarization mismatch [21]. In general, CP radiation could be realized if the antenna has two orthogonal modes with the same amplitude and a phase difference of 90° [5], pg. 830.

Various techniques for different types of antennas have been proposed to achieve circular polarization in the millimeter-wave band. For microstrip antennas, techniques such as trimming corners [51], adding tabs [16], and U-slot [40] have been utilized to generate circularly polarized radiation. Moreover, for CP cavity antennas, various shapes of cavities have been introduced, such as hexagonal cavity with truncated corners [17] and tapered-elliptical cavity [4]. However, most of those works have a narrow AR bandwidth. A way to address this issue is to introduce the concept of the ME dipole [28].

Different configurations [26] [12] [28] have been proposed to realize CP radiation on ME dipole antennas in millimeter band. In [26], the author realized CP radiation on a LP ME antenna by truncating a pair of electric dipole and adding a hook-shaped strip to another pair. This antenna has achieved wide impedance and AR bandwidth of 56.7% and 41%, respectively. However, this antenna was fed by a conventional L-shape probe which leads to a complicated manufacturing process. In [12], a compact coaxial fed CP ME dipole antenna with SIW feeding network was proposed. The antenna utilizes a pair of rotational symmetrical lighting-shape patches as an electric dipole to generate CP radiation and is excited by an L-shape feeding structure consisting of a rectangular stub and an inner conductor of the coaxial connector which is a part of SIW to coaxial transition. The antenna has achieved an impedance and AR bandwidth of 24.2% and 16.5%, respectively. In [28], the author proposed a CP aperture-fed ME dipole antenna with SIW feeding network, which contains two pairs of patches as electric dipoles. This antenna realizes CP radiation by connecting the two diagonally positioned patches using a metallic strip above the aperture. The antenna has achieved wide impedance and axial ratio bandwidth of 28.8% and 25.9%, respectively, at 60GHz. A common drawback to their works is the high profile; they both follow the original guideline proposed in [29] and utilize substrates with a height of roughly quarter wavelength which becomes a major issue when integrating the antenna into a front-end system. A low-profile wideband CP ME dipole antenna is in high demand.

Different techniques have been proposed to lower the profile of a LP ME dipole antenna. At lower frequency, the ME dipole antenna could reduce its thickness by folding the magnetic dipole [14] [13] and inclining the vertical walls [30]. However, these methods cannot be simply adapted for antennas fabricated on the printed circuit boards(PCB) due to the manufacturing complexity. In [24], the author proposed to use H-taper ground to lower the height to 0.11 λ_0. But this method still requires four layers of PCBs, which significantly increases the cost and manufacturing complexity. In 2020, [42] proposed an alternative way to reduce the thickness of a ME dipole antenna. The authors introduced two pairs of parasitic patches on the sides of the electric dipole. The slot feeds the electric dipole, and the dipole, in turn, drives four patches. The author succeeded in reducing the thickness of the antenna to 0.07 λ_0 and increasing the bandwidth at the same time.

Comparing to the LP ME dipole antennas, only a few studies on low-profile wideband CP ME dipole antennas are conducted in the millimeter band. In [49], Xu et al. replaced the straight arms of the LP ME dipole antennas with two L-shape patches, similar to works [37] [21], to generate orthogonal fields on the electric dipole with a low profile feeding network. However, the antenna still has a thick substrate with a height of 0.25 λ_s and a limited AR bandwidth of 8.29%. Very recently, [53] introduced a low profile CP antenna with two L-shape patches acting as the electric dipole and hexagonal parasitic patches at the time of writing this thesis and achieved a thin substrate of $0.15\lambda_s$ and an overlapped bandwidth of 16.3%. It should be noted that antennas demonstrated in this thesis were already developed before its publication and achieves a lower profile of $0.1\lambda_s$.

Different feeding methods such as L-shape probe [26] and aperture [28] have been utilized to excite the ME dipole antenna in millimeter band. Among them, the aperture coupling is easier to manufacture [54]. Moreover, the slot could also introduce additional resonant frequency, which could further increase the bandwidth. For SIW feeding networks, [1] demonstrates two potential positions of the slot: longitudinal and transverse, as shown in the Figure 2.9. The longitudinal slot requires an additional matching post in the substrate. However, it could provide wider bandwidth comparing to the transverse slot [1].

2.4 Circularly Polarized Antenna Array

Due to the shorter wavelength, mmWave antennas experience higher propagation loss than those in lower frequencies [2]. As a result, a single mmWave antenna often cannot fulfill the practical requirements, and an array of multiple antenna elements is required to improve the overall antenna performance. There are no strict rules on how to position

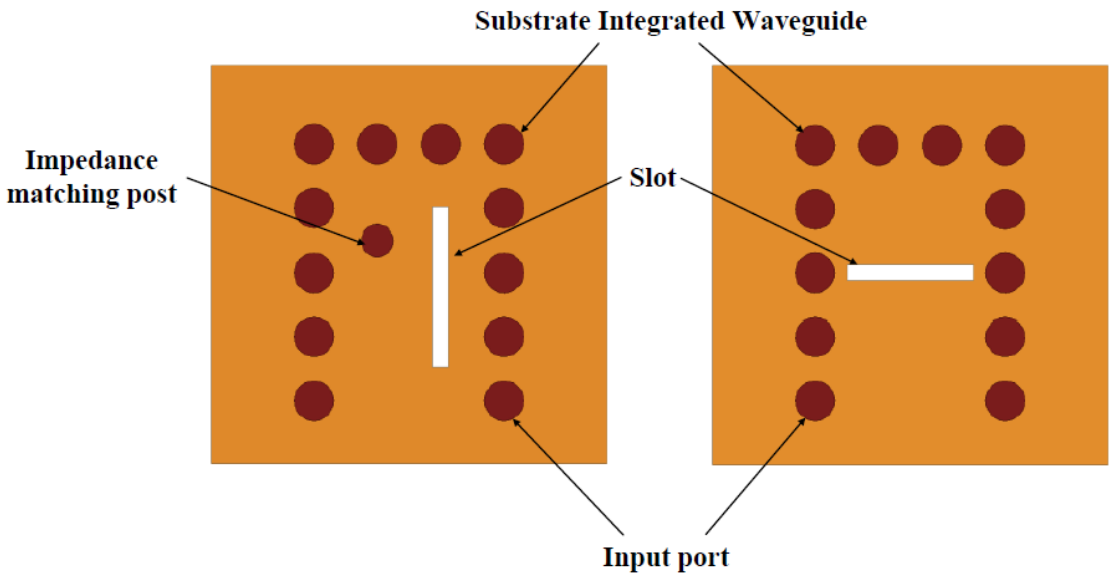

Figure 2.9: Different coupling aperture for a SIW Longitudinal(Left) Transverse(Right), adopted from [54]

elements inside an array. But in general, according to [5], pg. 285-286, the following factors need to be considered when designing an array: the overall physical layout of the array (linear, circular, etc.), separation distances between elements, and the phase and amplitude of excitation at each element, and the characteristic of a single antenna element such as radiation pattern and bandwidth.

Various circularly polarized antenna array has been proposed in the past and can be divided into three categories based on the polarization of the antenna elements and their feeding networks: LP elements with sequential rotated feeding network, CP elements with sequential rotated feeding network, and CP elements with uniformly distributed feeding network [54].

The sequential rotated technique (SRT) [20] was introduced by J. Huang to generate circularly polarized radiation from LP elements by arranging them with an angular orientation and feed phase difference of 90° from neighbor elements. Figure 2.10 from [20] illustrates the two basic CP array arrangements using sequential rotated feeding technique, where ψ indicates both angular orientation and feed phase of the LP element. As identical LP elements generate an electric field vector orthogonal to their neighbors with the same amplitude and a phase difference of 90°, both arrays are expected to create circularly polarized radiation.

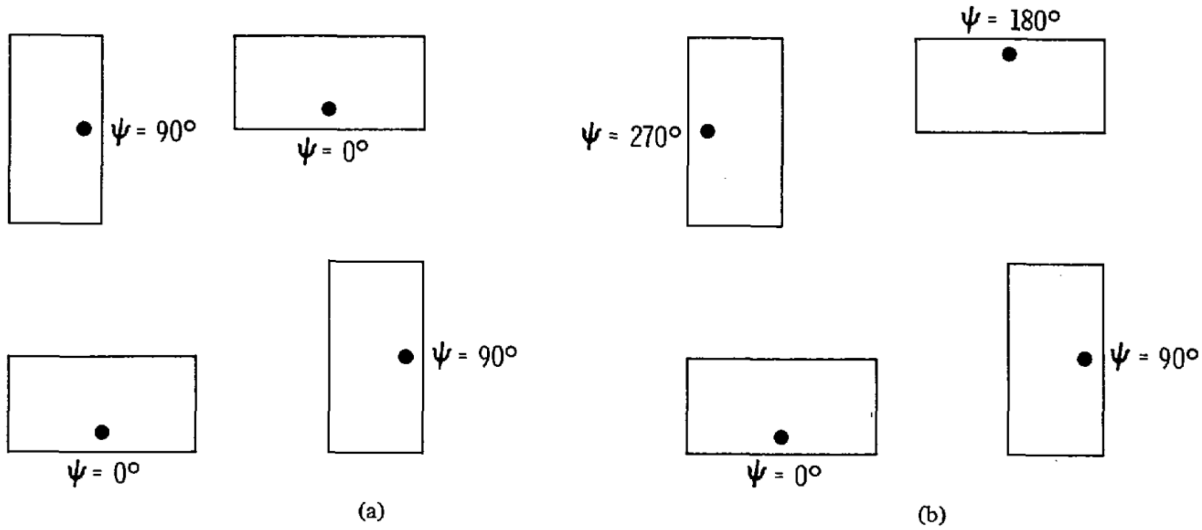

Figure 2.10: 2x2 microstrip arrays using sequential rotated technique, adopted from [20]

This technique has been used broadly in the millimeter band. In [15], D. Guan et al. proposed a 16x16 CP cavity-back slot antenna arrays using a SIW feeding network with SRT and achieved an AR bandwidth of 13.8%. The work utilizes a 2x2 subarray consisting of 4 LP cavity-back slot antennas as a basic building block and arranges them into a sequential rotation order with a phase difference of 90°. In [48], J. Xu et al. proposed a dual CP antenna array realized by sequential rotating subarrays consisting of LP SIW-fed patches and achieved a 2-dB AR bandwidth of 8.89% for both polarizations. The SRT has also been applied to arrays with CP elements to further increase their AR bandwidth.

In [43], the authors proposed a 1x2 CP array with CP ME dipole elements arranged by a difference of 90° and a sequential SIW feeding network realized by one phase delay line. The antenna array achieves a wide AR bandwidth of 24.7% despite its elements only have a limited AR bandwidth of 9.7%. In [12], the authors proposed a 4x4 CP antenna array consisting of CP ME dipole antenna elements and a sequential rotated feeding network; this work utilizes 2x2 subarrays as a basic building block and arranges them with a sequentially rotated angle of 90°. The final antenna array improves AR bandwidth from 16.5% of a single element to 27.8%. However, a sequential rotated feeding network often requires a complicated design and manufacturing process and a large area for implementation [47].

A simpler way to design a CP array is to utilize uniformly distributed feeding networks that feed each antenna element with the same amplitude and phase. However, without the help of the SRT to improve AR performance, this method generally requires wideband elements. In [28], an 8x8 CP antenna array with a full-corporate SIW feeding network based on a wideband CP ME dipole element was proposed and achieved a wide AR bandwidth of 16.5%. In [49], the authors constructed a 2x2 CP antenna array and a low-profile full-corporate feeding network using microstrip lines. The array has achieved an AR bandwidth of 11.33%.

Chapter 3

Low-profile Wideband Circularly Polarized Aperture-Fed ME Dipole Antenna with Parasitic Patches

Circularly polarized antennas have attracted more attention due to their ability to suppress multipath loss and polarization mismatch loss [21]. Various CP ME dipole antennas [26] [28] have been proposed in the past. However, there is one common drawback to their works, thickness. As most of the works follow the original guidelines proposed in [29], they utilize substrates with a height of a quarter wavelength which limits the antenna applicability.

In this chapter, a novel low-profile wideband circularly polarized ME dipole antenna with parasitic patches is proposed. To verify the performance of the antenna element, an antenna prototype with additional transmission lines and walls has also been designed, fabricated, and measured. The design of antennas is aided with the help of a 3D full-wave electromagnetic (EM) solver Ansoft HFSS [3].

3.1 Geometry

The geometry of the proposed circularly polarized ME dipole antenna with parasitic patches is shown in the Figure 3.1. The antenna comprises two layers of substrates made of Roger 5880 with a height of 0.787mm, a dielectric loss tangent of 0.0009, a relative permittivity of 2.2, a size of 10.7mm x 10.7mm (1 λ_0 x 1 λ_0 at 28GHz). A short-ended SIW feeding network is designed in the bottom layer. A longitudinal slot is etched on the upper ground plane of the SIW to feed the radiating element, and a matching post is also added in the bottom layer to improve the impedance matching. The radiating element is implemented in the second layer. Two inverted L-shape patches working as an electric dipole are placed on the top of the second layer and shorted by the two metalized vias embedded in the substrate. To improve both 3dB axial ratio and impedance bandwidth, four parasitic patches are added near the electric dipole, inspired by [42]. The detailed dimension of the antenna element is shown in Table 3.1.

Table 3.1: Dimension of the proposed antenna element (unit:mm)

Parameter	*A*	*P1*	*P2*	*B1*	*A1*	*C1*	*C2*	*C3*	*C4*	*R1*
Value	5.85	1.3	1.17	0.65	4	3.8	1.4	1.85	2.45	0.15
Parameter	*D1*	*L1*	*L2*	*L3*	*L4*	*SS1*	*SS2*	*SS3*	*P*	*R3*
Value	1.75	1	0.425	2.06	1.7	0.1	1.205	0.15	2.65	0.42
Parameter	*h1*	*h2*	*R2*							
Value	0.787	0.787	0.35							

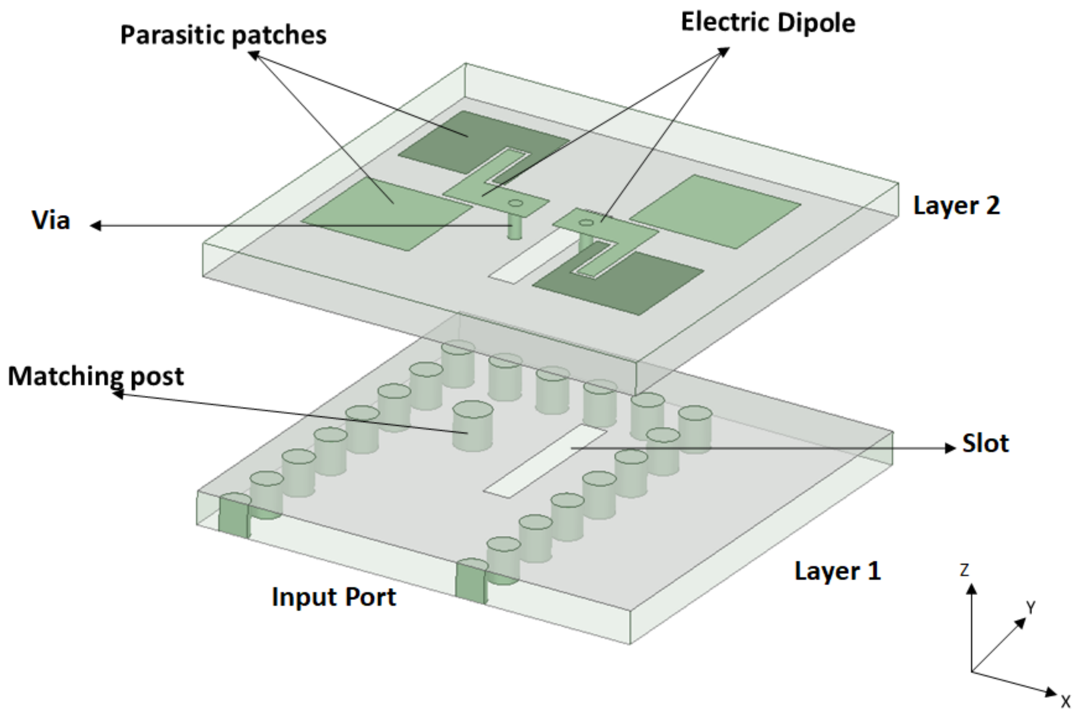

(a) 3D View

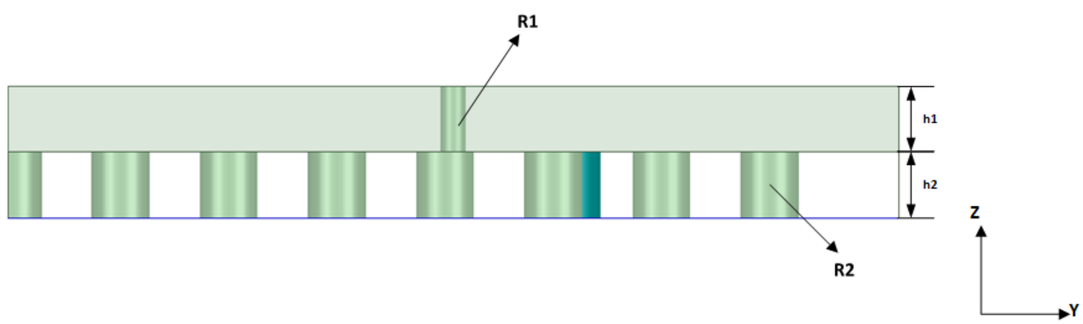

(b) Side View

Figure 3.1: Geometry of the proposed antenna element

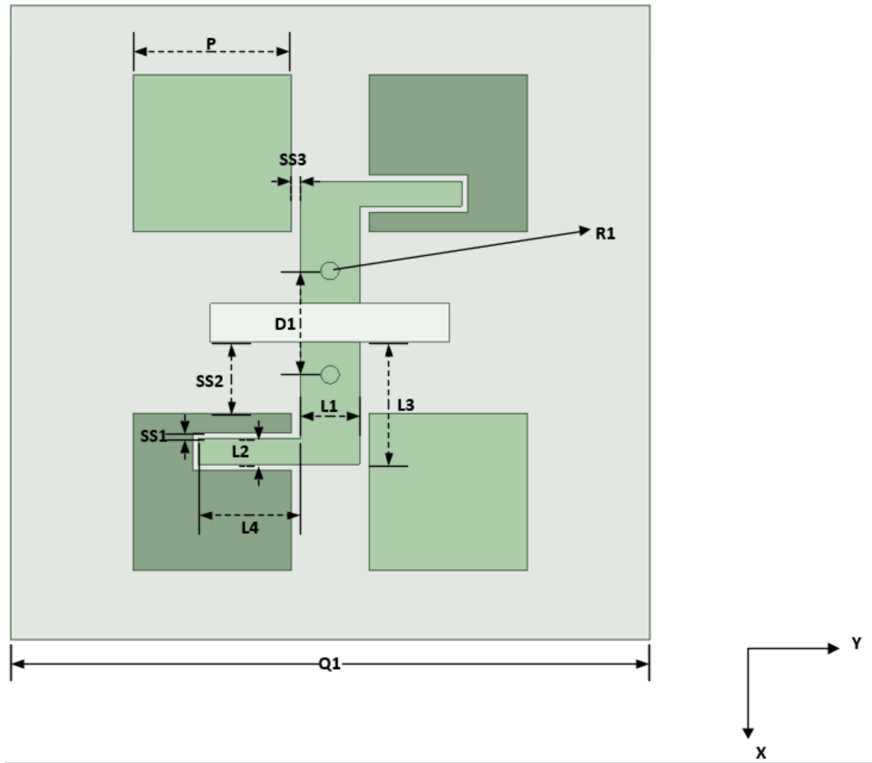

(c) Top View of the top layer

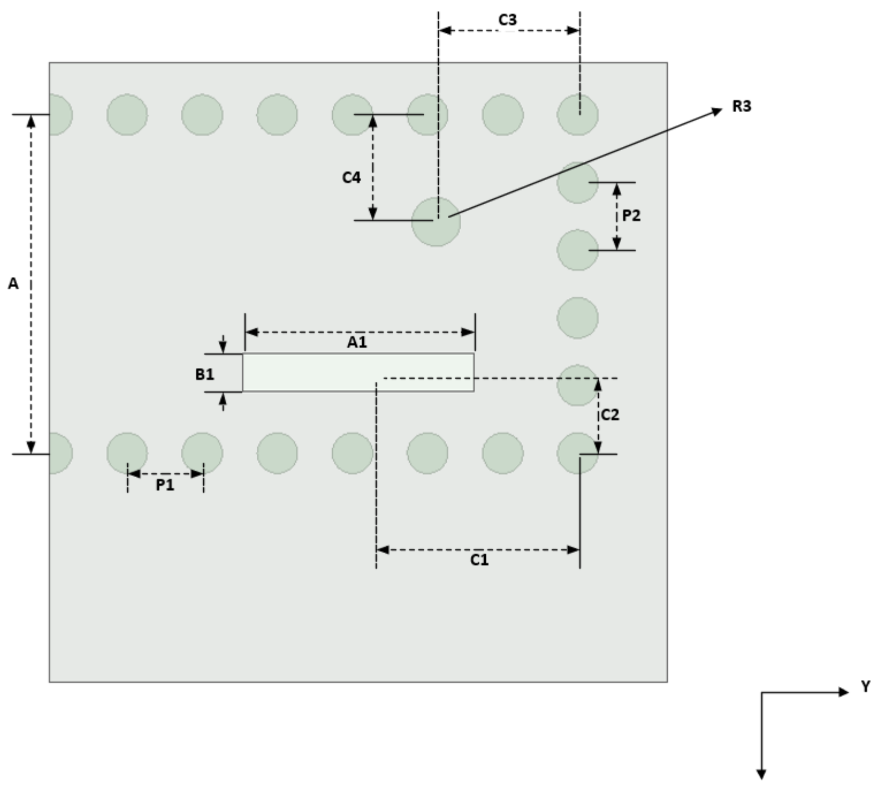

(d) Top View of the bottom layer

Figure 3.1: Geometry of the proposed antenna element (cont.)

3.2 Design Process

The entire design process of the proposed antennas is shown in the Figure 3.2. The design process starts with a basic aperture-fed linear polarized ME dipole antenna based on [42]. This basic antenna consists of a pair of shorted rectangular patches acting as an electric dipole and a magnetic dipole realized by the aperture between patches as shown in the Figure 3.2a. The bottom substrate contains the SIW feeding network, which follows the same dimension as calculated in the last chapter with a matching post. The height of the two substrates is set to be 1.8mm or $0.25\lambda_s$, where $\lambda_s = \lambda_0 / \sqrt{\epsilon_r}$, following the conventional guideline proposed by [29].

By replacing the original rectangular electric dipole with two rotational symmetric inverted L-shape patches similar to ones used in [12], the electric dipole generates rotational electric field on their surface and radiate circularly polarized waves. The structure of this antenna is shown in the Figure 3.2b. The width and length of the two arms and the slot are adjusted to maximize the overlap bandwidth. The result has been posted in the Figure 3.3a and 3.3b. This simple structure has achieved overlapped bandwidth of 9.8%(from 27.86GHz to 30.74GHz) which are comparable to the recently published CP ME dipole antennas works [43] and [49] which have overlapped bandwidth of 9.7% and 8.29% respectively.

However, there are two drawbacks to this reference design: narrow AR bandwidth and thick substrates. To achieve low profile and expand the bandwidth, the parasitic patches have been added close to the electric dipole and the slot have been readjusted while reducing the height of substrates by half. As shown in Figure 3.3a, and 3.3b, those

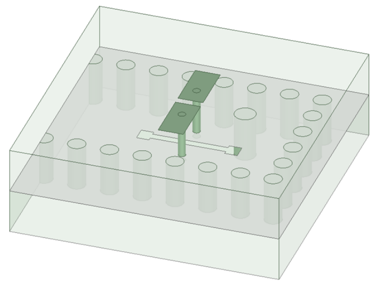

(a) LP ME Dipole Antenna

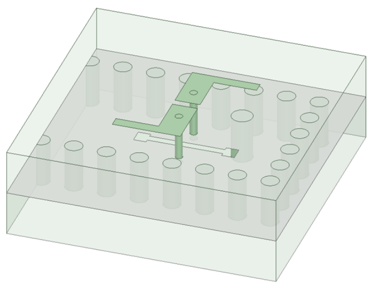

(b) CP ME Dipole Antenna(Reference)

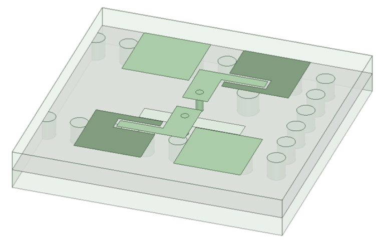

(c) Proposed Antenna

Figure 3.2: Design process of the proposed antenna element

changes do not only reduce the height of the antenna but also significantly improve the performance of the reference antenna element.

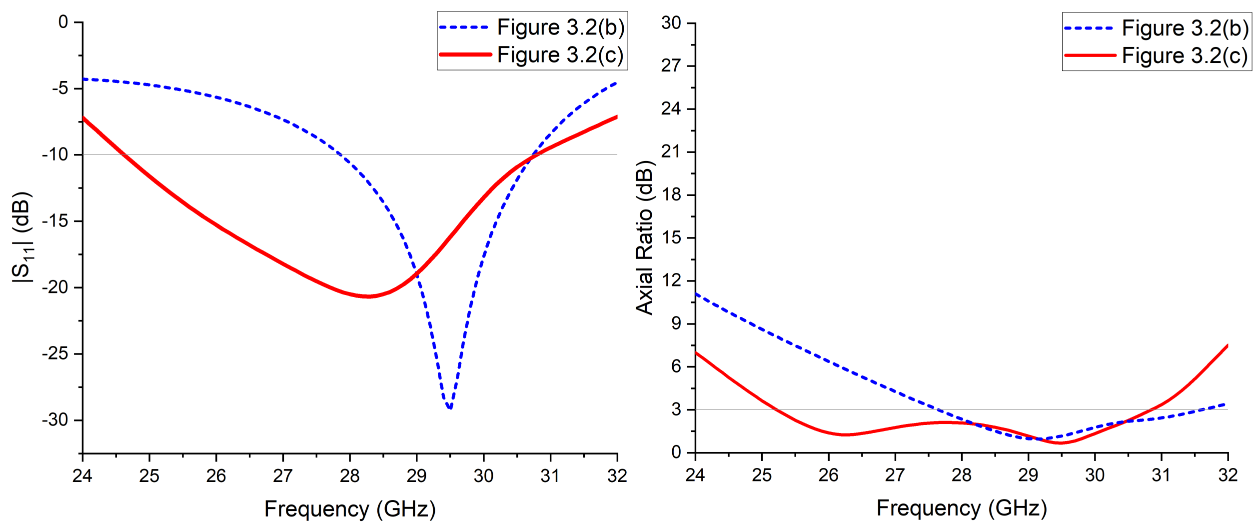

(a) **(b)**

Figure 3.3: Simulated (a)$|S_{11}|$ and (b)AR of the reference CP ME antenna and the proposed antenna

3.3 Operating Principle

The current distributions on the electric dipole and parasitic patches in one period of time, T, at two AR resonant frequencies, 26.2GHz and 29.5GHz, are shown in the Figure 3.4 and 3.5 respectively to illustrate the circular polarization generation process. At the lower frequency, 26.2GHz, the radiation is mainly contributed by the electric dipole, and the sum of current vectors flows along the direction of φ=315° at t=0. At t=T/4, the radiation is contributed by both parasitic patches and electric dipole. The current on the patches flows mainly in the negative y-direction, while the current on the electric dipole flows in the negative x-direction. By combining the current vectors, the sum of the current vector flows along the direction of φ=225°. At t=T/2 and 3T/4, the sum of the current vector has a similar amplitude as those at t=0 and T/4, respectively but flows in the opposite directions.

At $t = 0$ in the higher frequency, 29.5GHz, the radiation is contributed by the electric dipole together with top-left and bottom-right patches. As the current vector flows along the positive y-direction on the patches and positive x-direction on the electric dipole, the sum of the current vector flows along the direction of φ=45°. At t=T/4, the radiation is mainly contributed by the electric dipole and the sum of the current vector flows along the direction of φ=315°. At t=T/2 and 3T/4, the sum of the current vector has a similar amplitude as those at t=0 and T/4, respectively, but moves in the opposite direction.

With two orthogonal modes with similar amplitude and a phase difference of 90° at both resonant frequencies, circularly polarized radiation contributed by both parasitic patches and electric dipole could be expected. Furthermore, as the current vector rotates clockwise in one period of time, the co-polarization for this antenna is left-hand circular polarization (LHCP), and the cross-polarization is right-hand circular polarization (RHCP).

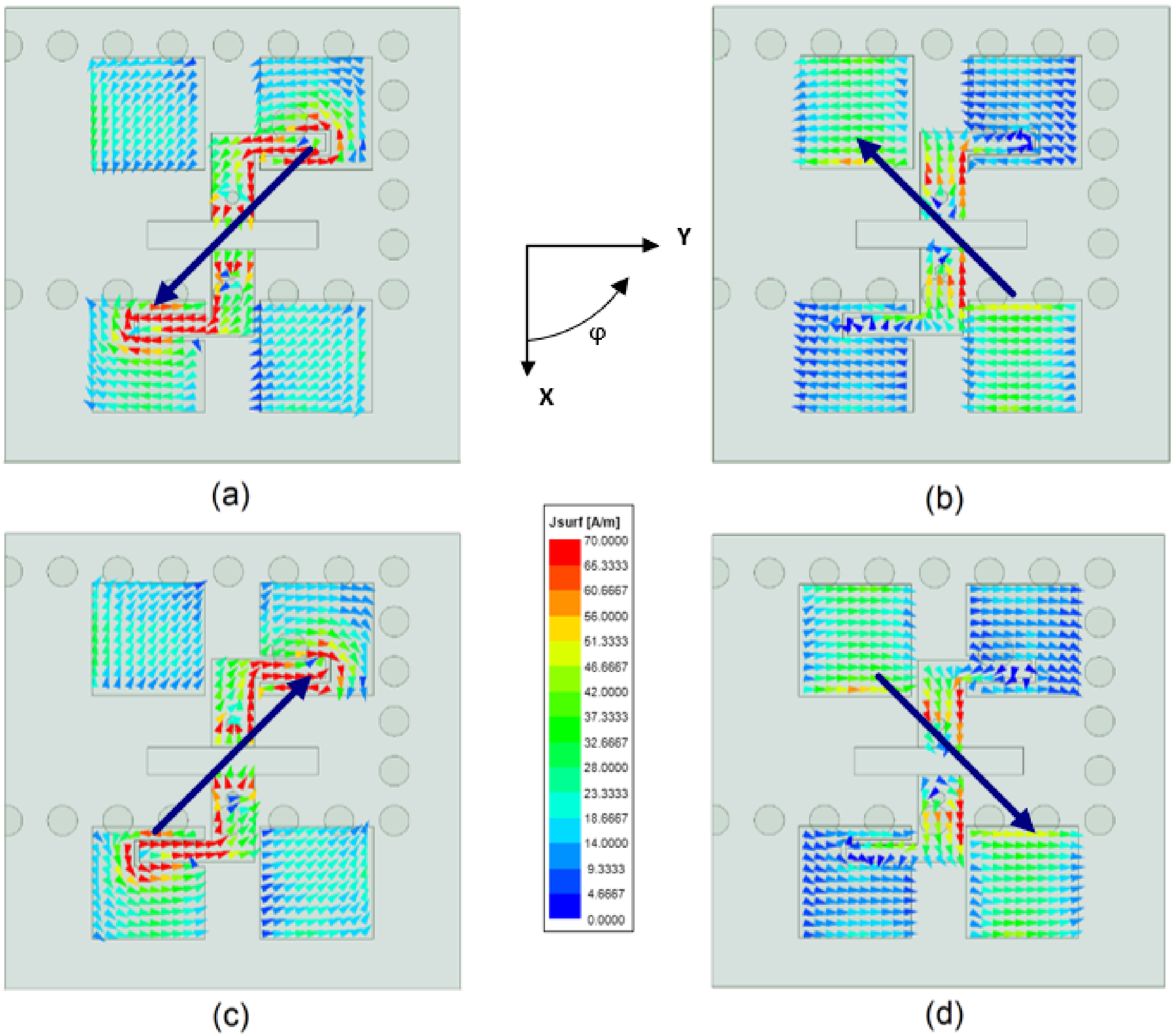

Figure 3.4: Current distribution of the proposed antenna element over a period of time at 26.2GHz (a) *t=0* (b) *t=T/4* (c) *t=T/2* (d) *t=3T/4*

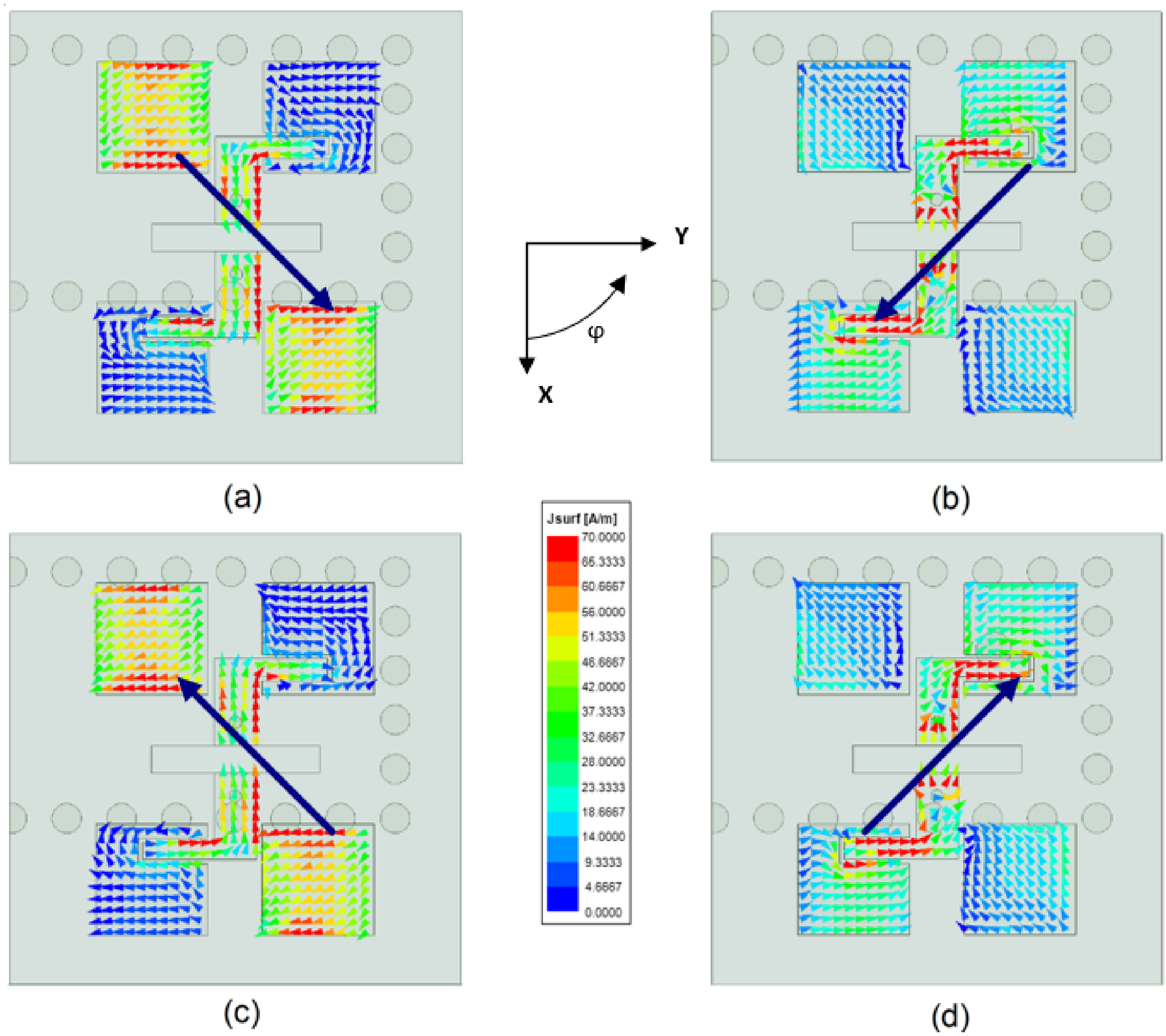

Figure 3.5: Current distribution of the proposed antenna element over a period of time at 29.5GHz (a) *t=0* (b) *t=T/4* (c) *t=T/2* (d) *t=3T/4*

3.4 Parametric Study

To better understand the working principle of the proposed antenna element, a series of parametric studies are conducted for the following key parameters: *SS2*, *SS3*, *P*, *B1*, and *L1*. All experiments are conducted with one independent variable at a time while all other parameters remain the same.

As shown in the Figure 3.6, with the decrease of *SS2*, the impedance bandwidth increases, and the first and second AR resonance frequencies tend to move toward the lower and higher frequency, respectively, which results in a wider AR bandwidth. However, it could be observed that the AR performance has been negatively affected in the middle of the bandwidth when two resonant frequencies are too further apart. The distance between the electric dipole and parasitic patches, *SS3*, plays a crucial role in the AR performance, as shown in the Figure 3.7. When the *SS3* decreases, two AR resonant frequencies move further apart, which increases the AR bandwidth. However, the AR performance drops significantly when the parasitic patches move too close to the electric dipole. The size of parasitic patches, *P*, is also important, as shown in the Figure 3.8. By decreasing the size of patches, the entire AR and impedance bandwidth shift to a higher frequency. The width of the slot, *B1*, has a substantial impact on the impedance bandwidth as shown in the Figure 3.9. By reducing *B1*, the entire impedance bandwidth shift towards the lower frequency. Furthermore, the width of the electric dipole has a significant influence on both impedance and AR bandwidth. As shown in Figure 3.9, with the increase of *L1*, the lower end of the impedance bandwidth moves toward the lower frequency, and the AR bandwidth improves dramatically. However, after reaching 1mm, *L1* has little impact on the AR performance.

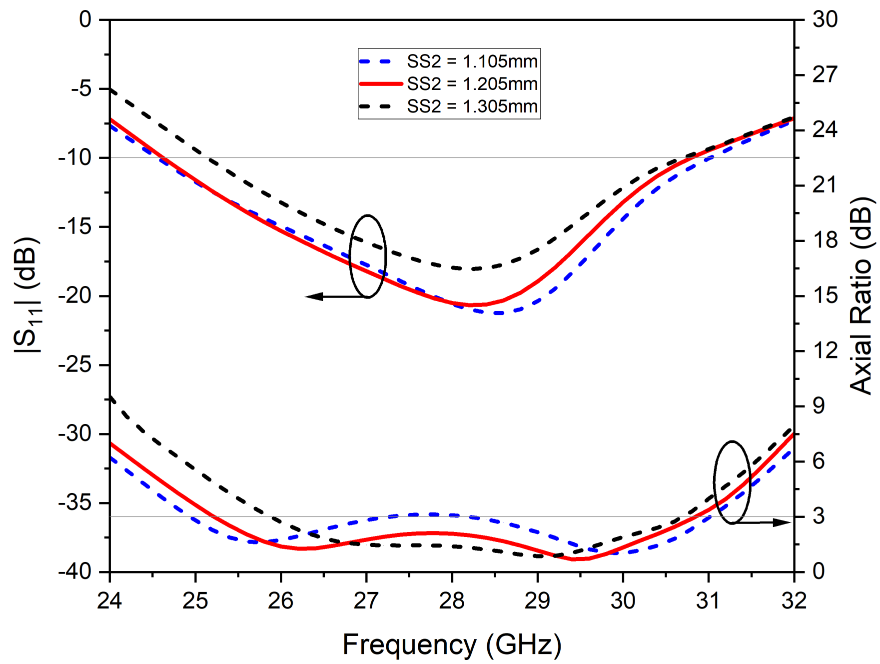

Figure 3.6: Simulated $|S_{11}|$ and AR of the proposed antenna with different SS2

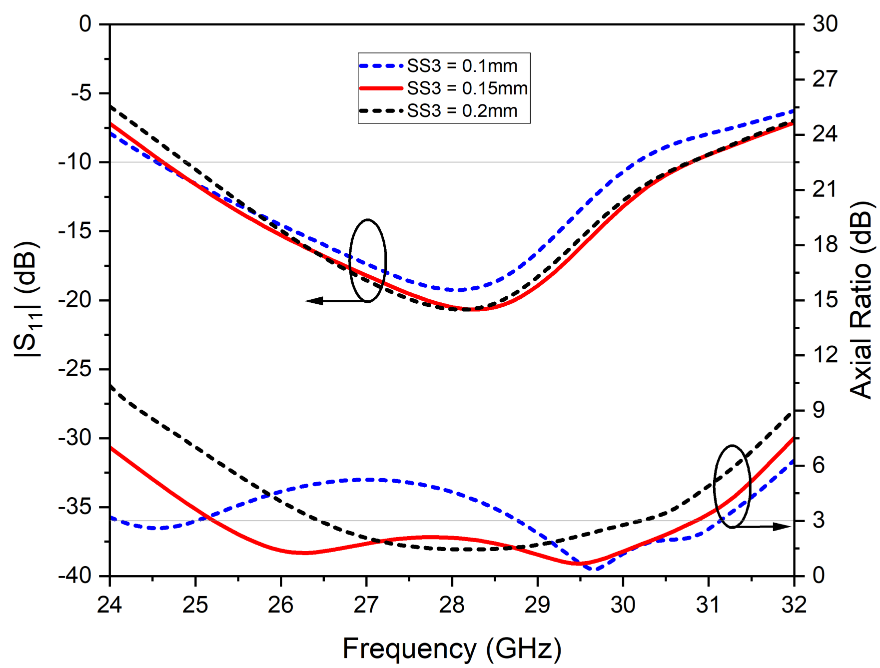

Figure 3.7: Simulated $|S_{11}|$ and AR of the proposed antenna with different SS3

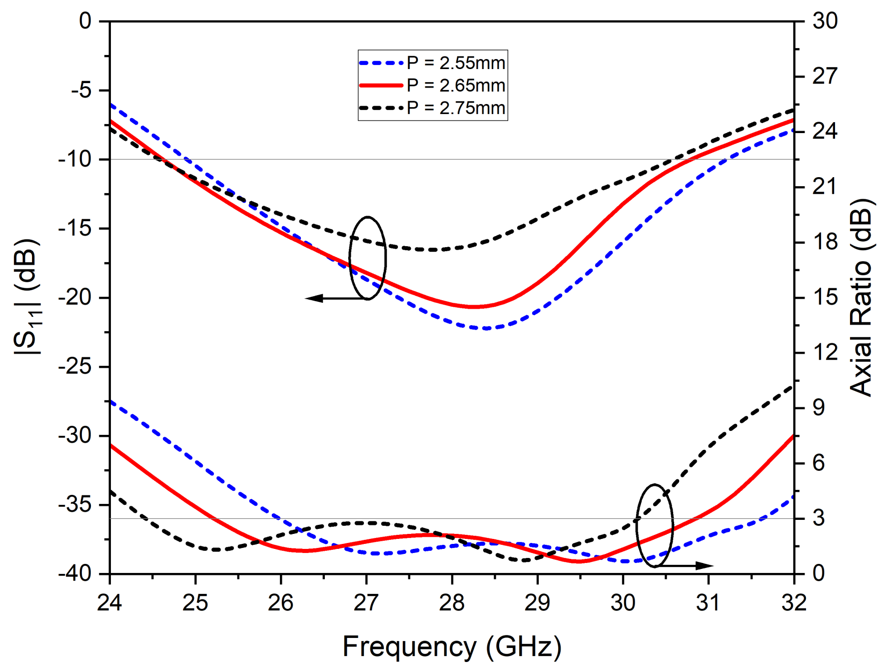

Figure 3.8: Simulated $|S_{11}|$ and AR of the proposed antenna with different P

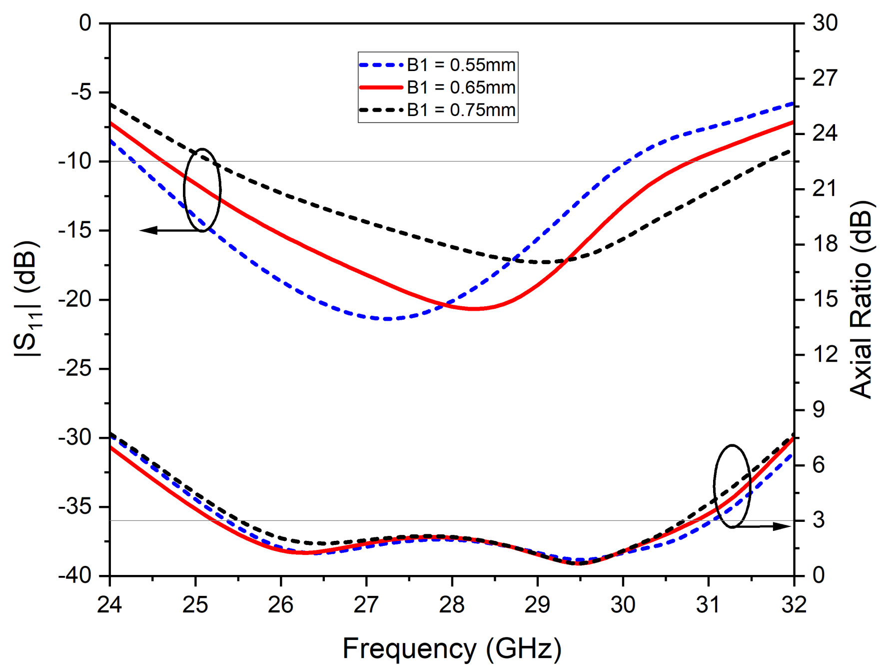

Figure 3.9: Simulated $|S_{11}|$ and AR of the proposed antenna with different B1

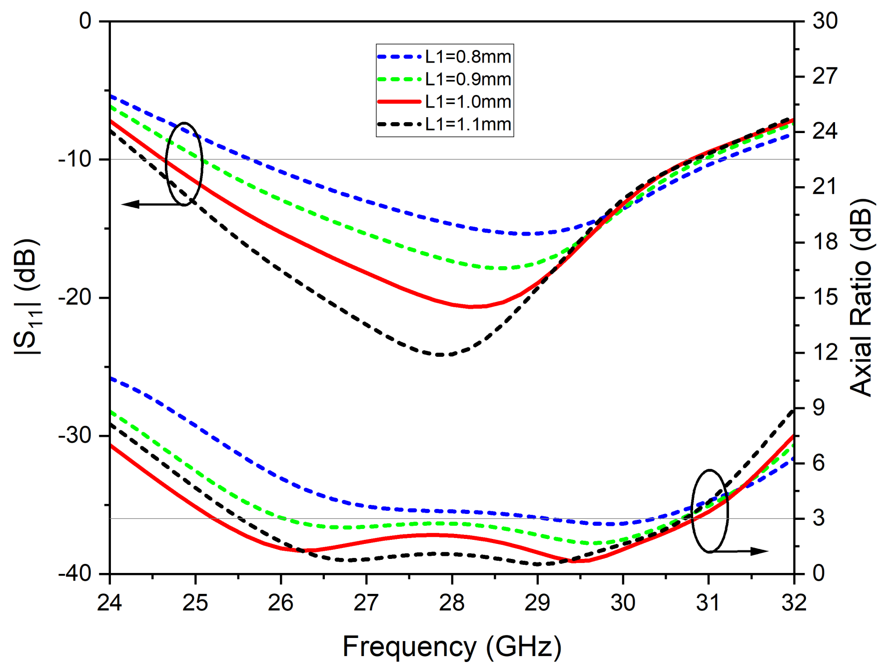

Figure 3.10: Simulated $|S_{11}|$ and AR of the proposed antenna with different L1

3.5 Performance

The figure 3.3a and 3.3b show the simulated $|S_{11}|$ and AR of the proposed antenna element respectively. The simulated impedance bandwidth is 22.1%(from 24.64GHz to 30.77GHz), and the 3dB AR bandwidth is 20.1%(from 25.22GHz to 30.85GHz). Comparing to the reference antenna, the overlapped bandwidth has increased dramatically from 9.8% to 19.8%, and the thickness of the antenna element has reduced from 1.8mm($0.25\lambda_s$) to 0.787mm (0.07 λ_0 or $0.1\lambda_s$). Within the overlapped bandwidth, the antenna has a simulated gain that varies in the range of 7.4 to 8.8 dBic as shown in the Figure 3.11b. The simulated radiation patterns of the *XOZ* plane and *YOZ* plane at 27 and 29GHz are shown in the Figure 3.12. The antenna element has achieved symmetrical cardioid radiation patterns with low cross-polarization level in both planes like other ME dipole antennas.

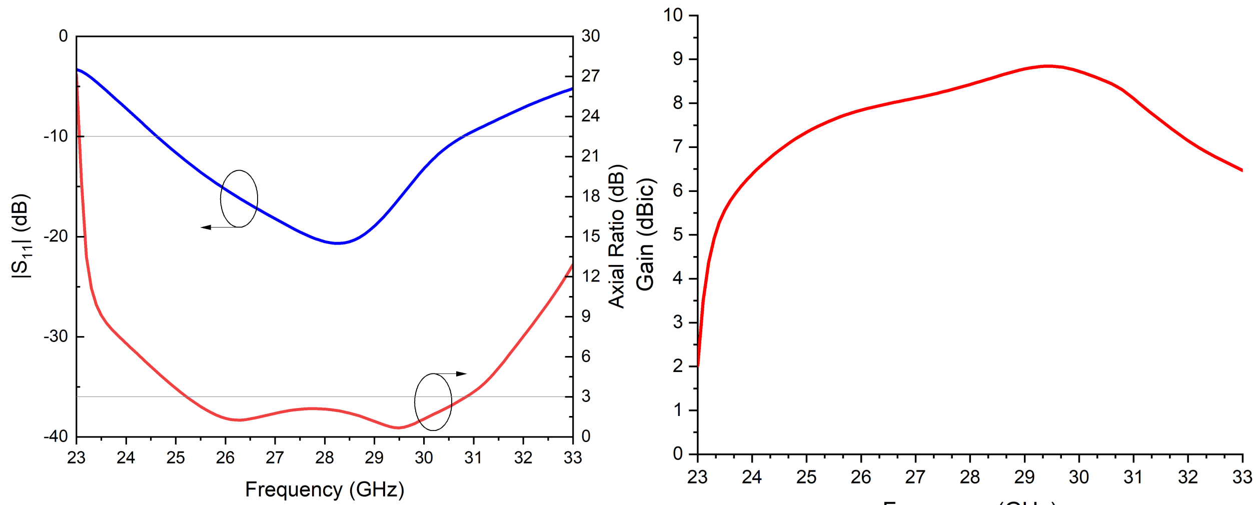

(a)

(b)

Figure 3.11: Simulated (a)S_{11}, AR and (b) gain of the proposed antenna element

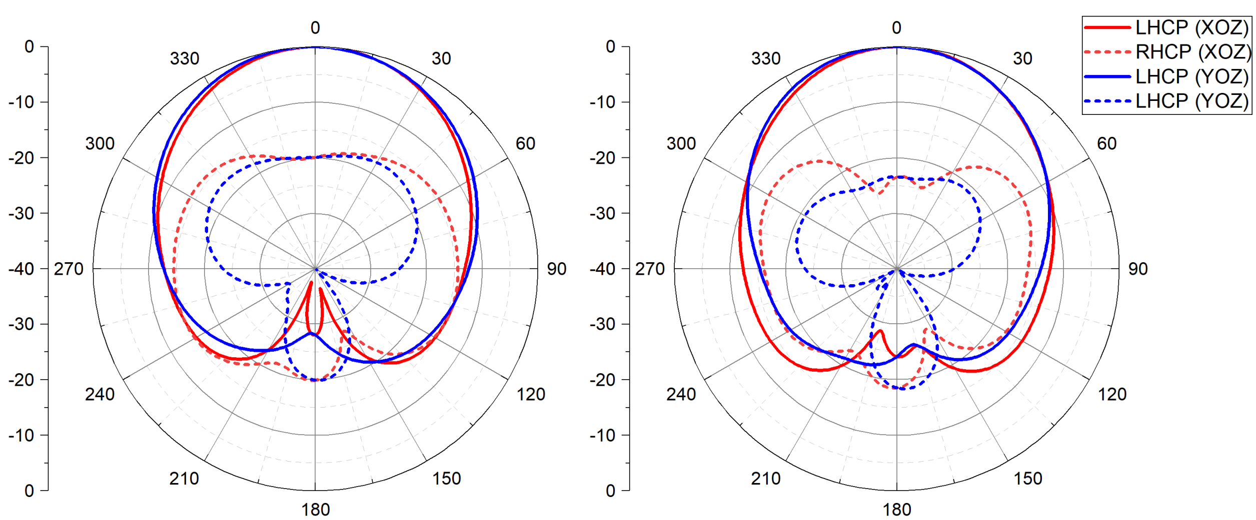

(a)

(b)

Figure 3.12: Radiation patterns of the proposed antenna element at (a)27GHz and (b)29GHz

3.6 Fabrication and Measurement

Due to the manufacturing constraints, it is not practical to feed the proposed antenna element with a waveguide connector directly. To verify the performance of the propose antenna element, an antenna prototype with additional transmission lines and walls has been designed, fabricated and measured, as seen in the Figure 3.13 and 3.14. The detailed dimension of the prototype can be found in the Table 3.2.

The 50-ohm microstrip line has been chosen as a transition between SIW and SMP connector to feed the antenna element due to its simplicity. To reduce the influence of the radiation from the microstrip line, the SIW has also been extended. Moreover, as the AR performance of a CP antenna could be easily affected by the change of the substrate and ground plane size, two walls, consisting of metallic posts and rectangular-shaped shorted patches, have been added to suppress the surface wave and further isolate the radiating element from the surrounding, as suggested by [54]. Figure 3.15 shows a performance comparison of prototypes with and without walls. Despite adding walls decreases the upper limit of AR bandwidth, it greatly improves the AR performance in the middle of the operating frequency band, which, in turn, increases the overall overlapped bandwidth of the prototype.

Table 3.2: Dimension of the proposed antenna prototype (unit:mm)

Parameter	*Lp1*	*Lp2*	*Lp3*	*Lp4*	*Lp5*	*Lp6*
Value	9.8	1	1.2	2.42	5.675	4.2

The antenna is fabricated using the standard single-layered PCB and plated-through-hole technologies, as shown in the Figure 3.16. And the top and bottom layers have been

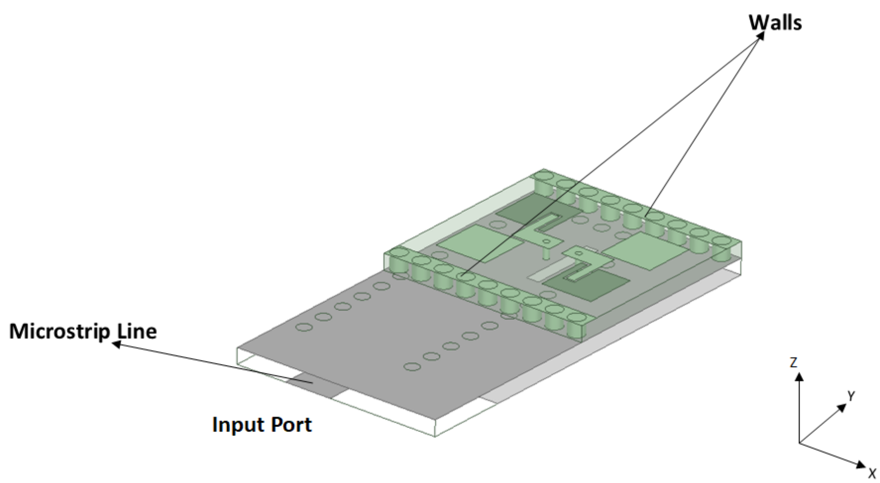

Figure 3.13: 3D View of the antenna prototype

bonded using silver conductive adhesives. The SMP connector is then connected to the end of the microstrip line to feed the antenna.

The $|S11|$ is measured using the Ceyear 3672D (10MHz to 50GHz), while other parameters are measured in a far-field anechoic chamber. The environment setup is shown in the Figure 3.17. The anechoic chamber is covered by the radio wave absorbing material to minimize the reflection of the EM waves and the interferences from other sources. A standard horn antenna is used to transmit the signal to the antenna under test (AUT). The distance between the horn antenna and the AUT is set to be $10\lambda_0$. Due to the limitation in the measurement environment, only the upper hemisphere (-90° to 90°) of the radiation pattern is considered in this thesis. The radiation patterns and AR are determined using the measured phase and amplitude of the orthogonal components. The antenna gain is calculated by comparing the difference between the maximum received signal strength of the AUT and a reference antenna.

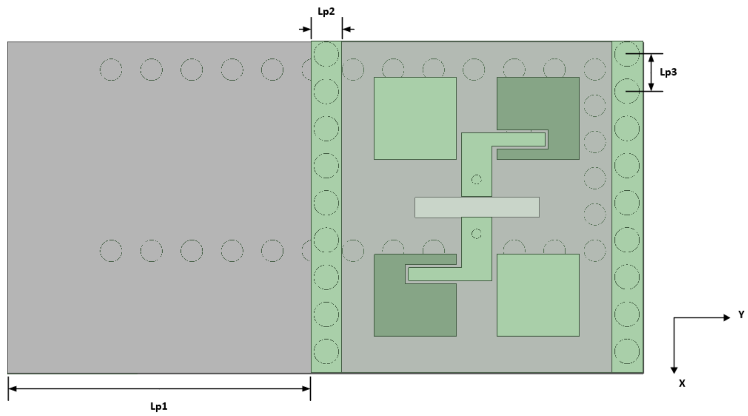

(a) Top view

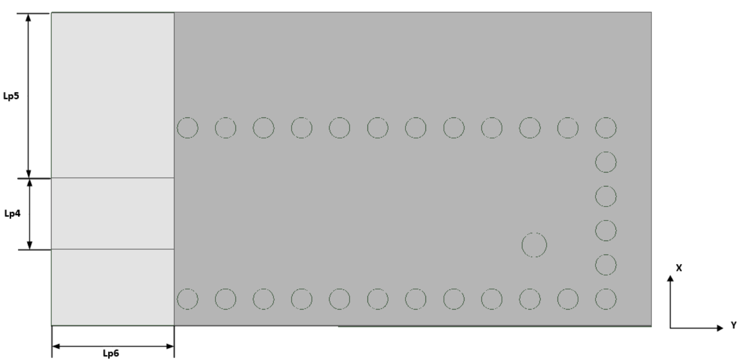

(b) Bottom View

Figure 3.14: Geometry of the proposed antenna prototype

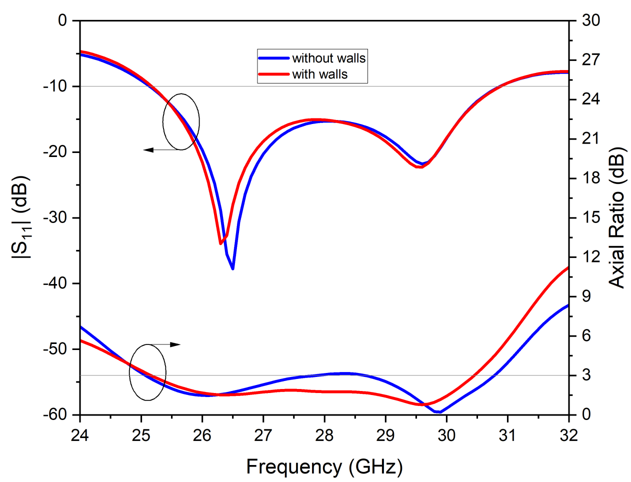

Figure 3.15: Simulated $|S_{11}|$ and AR of the proposed prototype with and without walls

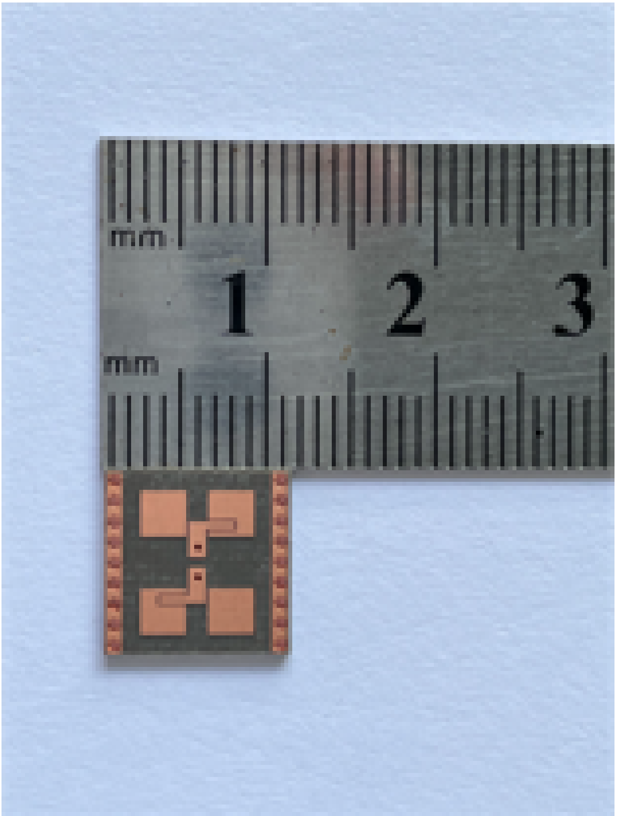

(a) Top layer

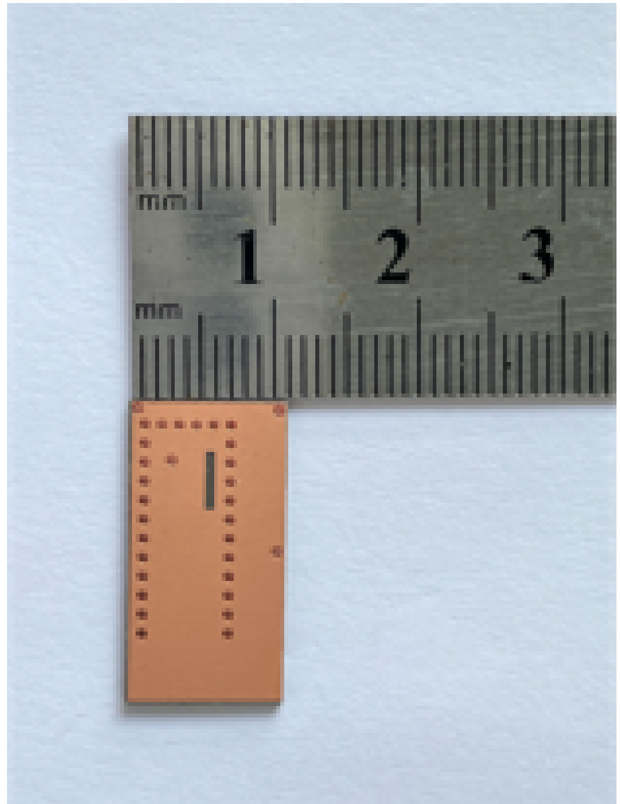

(b) Bottom Layer

Figure 3.16: Fabricated antenna prototype before assembly

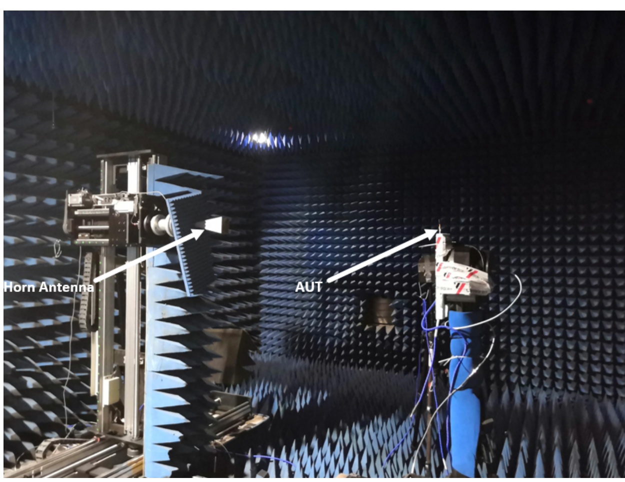

(a) Anechoic chamber

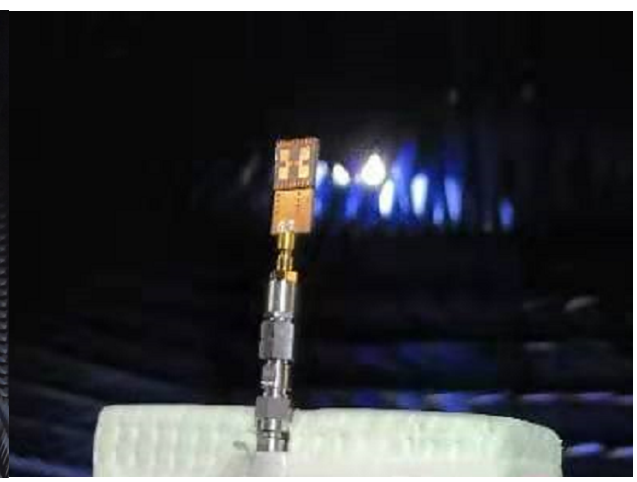

(b) Proposed antenna prototype

Figure 3.17: Far-field measurement system setup

3.7 Experimental Results and Discussion

With those modifications, it is expected for the antenna prototype to have different results compared to the single element alone. The simulated and measured results of the fabricated antenna prototype are shown in the Figure 3.18. The simulated and measured impedance bandwidth are 20.30%(from 25.18 to 30.87GHz)) and 19.65%(from 24.96 to 30.4GHz), respectively. The simulated and measured 3dB AR bandwidth are 19.03%(from 25.16 to 30.45GHz) and 17.49%(from 25.67 to 30.59GHz), respectively. Furthermore, the prototype has achieved a simulated and measured gain of 7.8 ± 1.2 dBic and 7.2 ± 1.1 dBic, respectively. Moreover, as shown in the Figure 3.19, the simulated and measured radiation patterns are in good agreement. The measured pattern has a slightly larger cross-polarization level; it is still within the acceptable range, which is less than -10dB, in the main direction. The deviation between simulated and measured results is mainly caused by the connector and fabrication error. A comparison between the proposed antenna prototype with other mmWave ME-dipole antenna elements is listed in the Table 3.3. The proposed antenna prototype has achieved a wide measured overlapped bandwidth of 16.87% while maintaining a low profile of only $0.1\lambda_s$.

Table 3.3: Performance comparison between the proposed antenna prototype with previous works in the millimeter band

Ref.	Overlap. BW	Peak Gain(dBic)	Element Thickness(λ_s)
[28]	25.9%	9.1	0.23
[50]	8.29%	6.97	0.23
[35]	21.9%	8.6	0.28
[12]	16.5%	n/a	0.2
This work(prototype)	16.87%	8.3	0.1

Overlap. BW is defined as the range of frequencies which have $|S_{11}| < -10dB$ and $AR < 3dB$

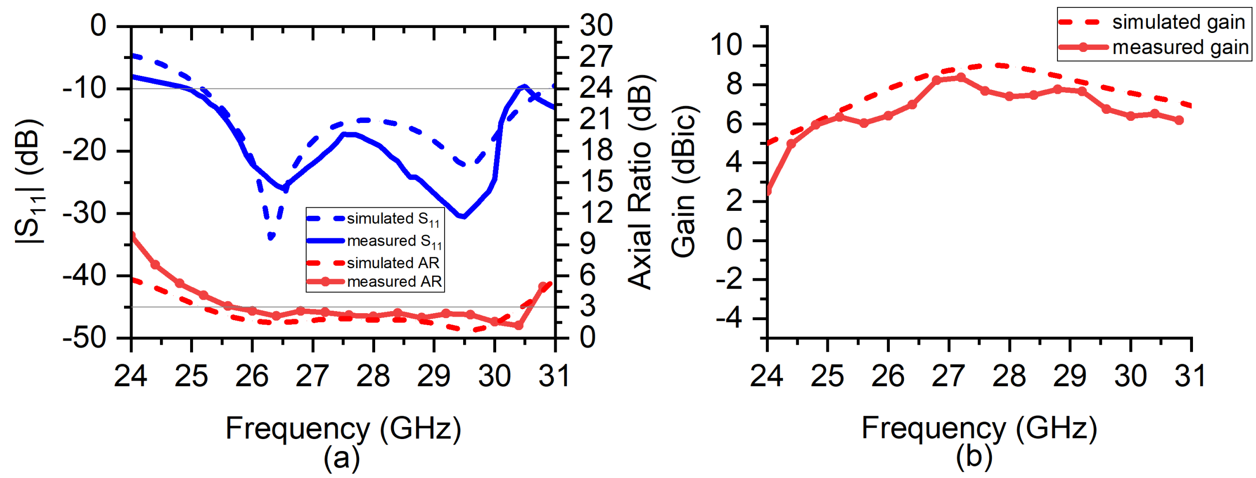

Figure 3.18: Simulated and measured (a) $|S_{11}|$, AR and (b) gain of the proposed antenna prototype

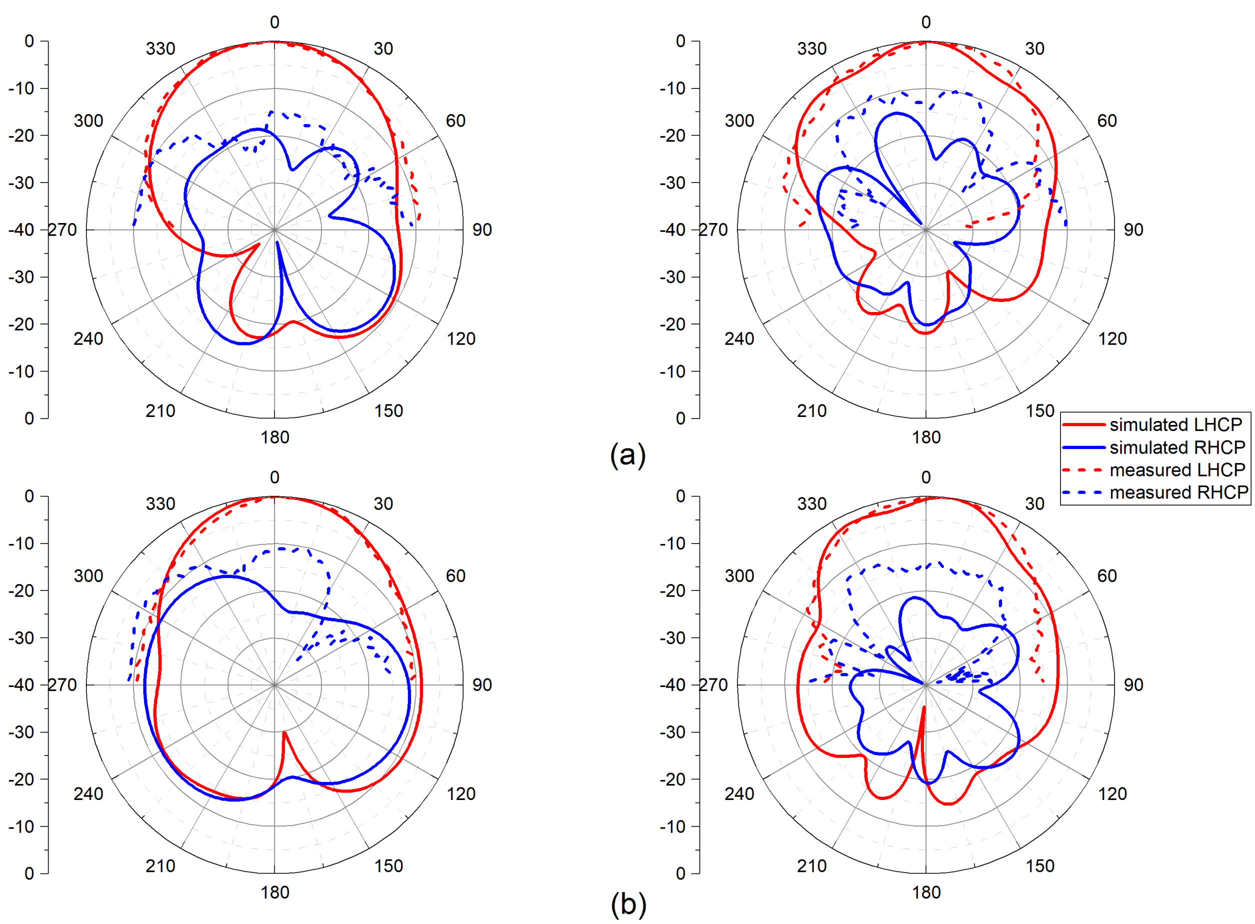

Figure 3.19: Simulated and measured radiation patterns of *XOZ* plane(left) and *YOZ* plane(right) of the proposed antenna prototype at (a)27GHz and (b)29GHz

Chapter 4

Linear Four Element Circularly Polarized ME Dipole Antenna Array

The mm-wave antenna experiences higher propagation loss in free space than those in lower frequencies. As a result, a single antenna element often cannot fulfill practical needs. A way to solve it is to arrange multiple antenna elements into an array to improve the overall gain.

Different structures of circularly polarized antenna array have been proposed in the past, such as CP/LP elements with sequential rotated feeding networks and CP elements with a uniformly distributed network. Among two different methods, the sequential rotated technique (SRT) has been used to improve AR performance. However, it requires a complicated and time-consuming design process and a large area for implementation. The uniformly distributed network, on the other hand, has a simpler structure comparing to ones with SRT, which significantly reduces the design and manufacture complexity, but its performance is greatly dependent on the performance of the individual element.

Due to the time and manufacture limitation, the uniformly distributed network with the same phase has been chosen as the feeding network for the design. Moreover, as the proposed antenna element has already achieved a wide AR bandwidth, it is able to achieve comparable AR performance without using the SRT. Furthermore, the SIW has also been utilized in the design instead of conventional transmission lines such as microstrip lines to reduce the transmission loss of the feeding network.

In this chapter, a four-element linear CP antenna array with a SIW feeding network consisting of a Wilkinson power divider [44], which equally divides power from one input port to four output ports with the same amplitude and phase, is designed, fabricated, and measured. The design of the antenna array is aided with the help of the HFSS.

4.1 Elements Spacing

As this chapter aims to design a linear array with a uniformly distributed network, the elements should be positioned along a single line with equal distance between them. Before designing the power-divider or feeding network, it is crucial to determine the desired separation distance between elements. In general, the elements should locate within one free-space wavelength from each other to avoid large sidelobe level (SLL). However, when the elements place too close to each other, the mutual coupling effect might negatively affect the antenna array performance. Moreover, due to the large space requirement of the substrate integrated waveguide, it is also essential to leave enough design space between elements.

To find the optimal distancing for the array, an experiment is conducted by positioning four antenna elements along the x-axis at various distances with a modified ground plane and two walls like the antenna prototype to suppress the surface wave and improve the AR performance. Due to the time constraints, only the simulation has been performed and four wave ports are used to excite the elements instead of a complete feeding network. The geometry of the element-only array is shown in the Figure 4.1.

Figure 4.2 shows the simulation results of the element-only array. The elements are placed at four separation distances, S: 9, 9.5, 10.5, and 11.5mm. The result indicates that the impedance bandwidth is less sensitive to the changes, while the AR performance has been affected considerably. The overlapped bandwidth has been improved greatly from 8.31% (25.48 to 27.69GHz) at 11.5mm to 16.9% (from 25.91 to 30.12 GHz) at 9.5mm. The performance has reached a plateau after 9.5mm; at 9mm, the array has only an overlapped bandwidth of 16.5% as the AR bandwidth continues shifting to lower frequency while the impedance bandwidth stays the same. Moreover, the SLL reaches the maximum value when the separation is at 11.5mm and decreases with the separation distance, which meets our expectations.

The separation distance of 9.5mm has been selected for our array. Even though the sidelobe level could be further reduced with a shorter distance, it has a better overlapped bandwidth among four separation distances. Furthermore, 9.5mm also provides a relatively larger design space for the power divider, which avoids the need for a multi-layer structure and reduces design and manufacturing complexities.

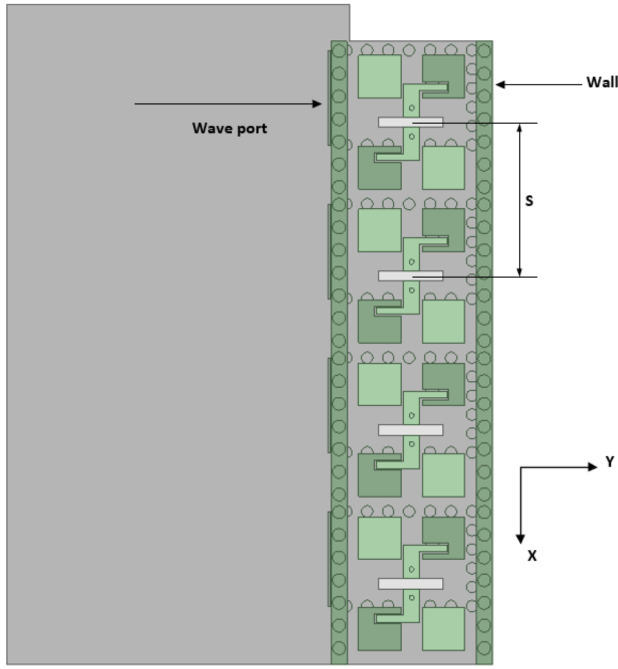

Figure 4.1: Geometry of the element-only array

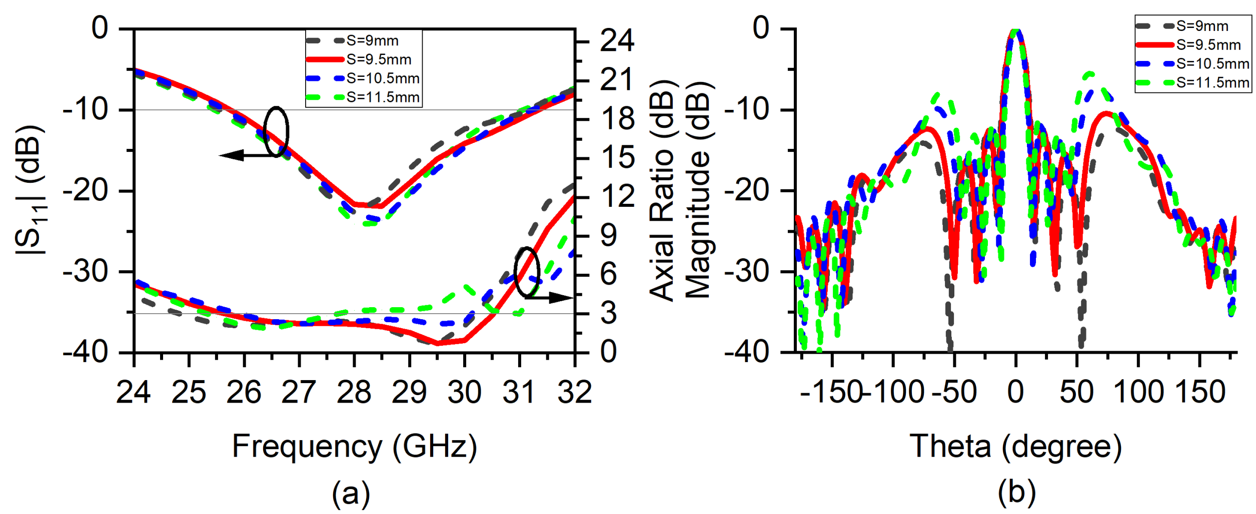

Figure 4.2: Simulated (a) $|S_{11}|$, AR, and (b) radiation patterns of XOZ plane at 29GHz of the element-only array with different spacing

4.2 Design of 1x4 Power Divider

The simplest way to feed antenna elements with the same amplitude and phase is to connect every single element with its own individual port. However, this method could dramatically increase the cost and space requirements when the number of components increases [7]. Instead, a power divider could be used to feed each element with desired phase and power.

A 1x4 corporate power divider has been designed using a single layer of Roger 5880. As shown in the Figure 4.3, the proposed power divider contains five ports (one input port and four output ports), three junctions, and multiple matching posts. The output ports have a spacing of 9.5mm between each other, as discussed in the previous section. To simulate the designed power divider, five wave ports have been added to each port; only one wave port at the input port is excited to feed the network while the other four wave ports are placed at output ports to verify the performance.

The simulated results can be found in the Figure 4.4. This power divider has an operating bandwidth from 25.68GHz to 31.52GHz. Within the bandwidth, four output ports have insertion loss ranged from -6.47 to -6.61 dB, and the difference between each port is less than 0.3 dB. Moreover, the phase of each output is displayed in the Figure 4.4b; the four lines are overlapped with each other, which indicates that all four ports have the same phase. In summary, this power divider could uniformly distribute power to each port with the same phase over the most operating bandwidth of the antenna element and entire overlapped bandwidth of the element-only array discussed in the previous section, which meets our design requirement.

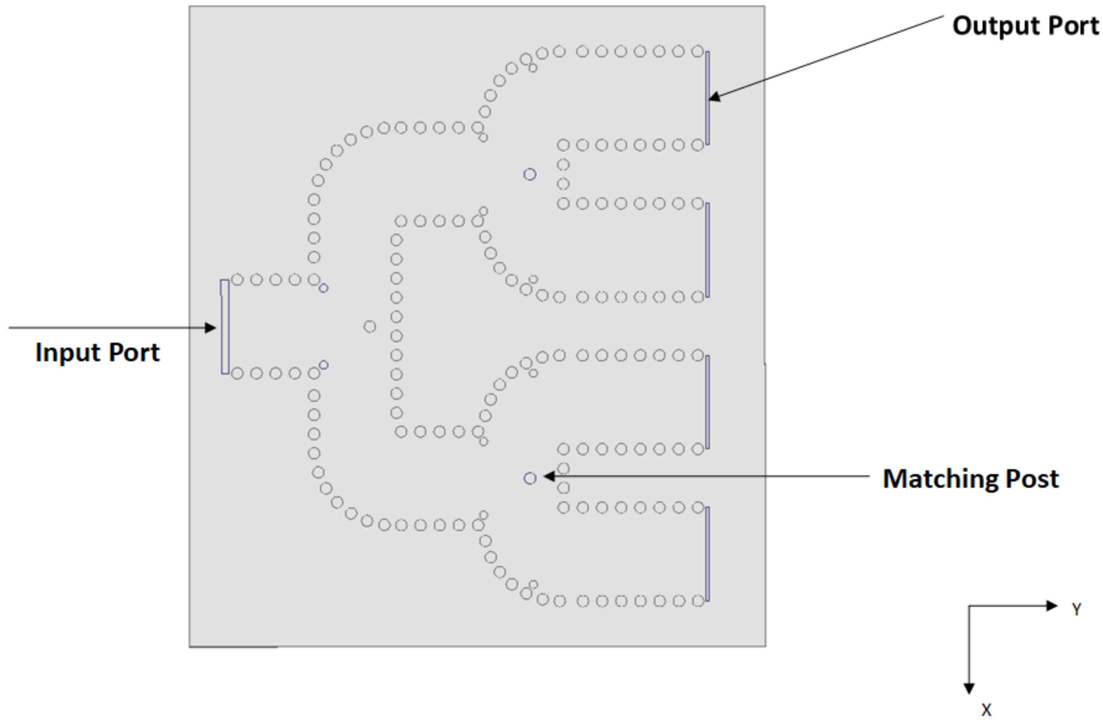

Figure 4.3: Geometry of the 1x4 power divider

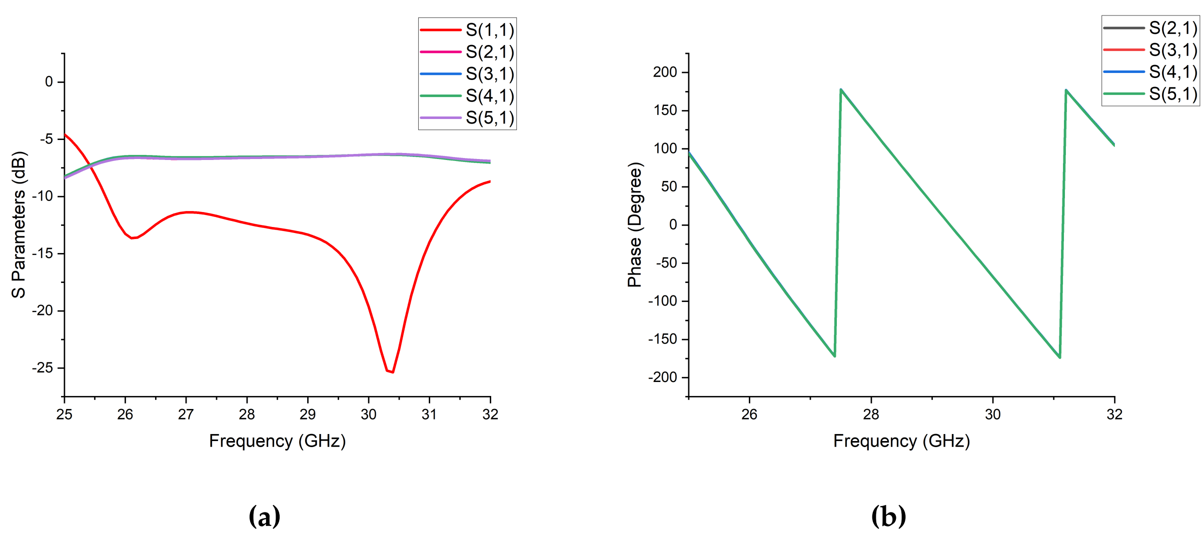

Figure 4.4: Simulated (a)S-parameters and (b) phase of output ports of the 1x4 power divider

4.3 Design of 1x4 Linear Array

In this step, four antenna elements have been connected to the outputs of the power divider with a spacing of 9.5mm or 0.88 λ_o. A 50-ohm microstrip line has also been added to use as a transition to the SIW network. Moreover, like the antenna prototype, two walls, which consist of metallic posts and rectangular-shaped shorted patches, have been used to suppress the surface wave and further isolate the radiating elements from the surroundings.

The antenna array has been constructed using two layers of Rogers 5880 with a height of 0.787mm, a dielectric loss tangent of 0.0009, a relative permittivity of 2.2. The geometry of the antenna array is shown in the Figure 4.5 and 4.6, and its detailed dimension is listed in the Table 4.1.

Table 4.1: Dimension of the proposed antenna array (unit:mm)

Parameter	*S*	*T1*	*D1*	*D2*	*D3*	*D4*
Value	9.5	1	5.85	5.15	1.65	2
Parameter	*D5*	*D6*	*D7*	*D8*		
Value	7.33	2.42	5.9	5.3		

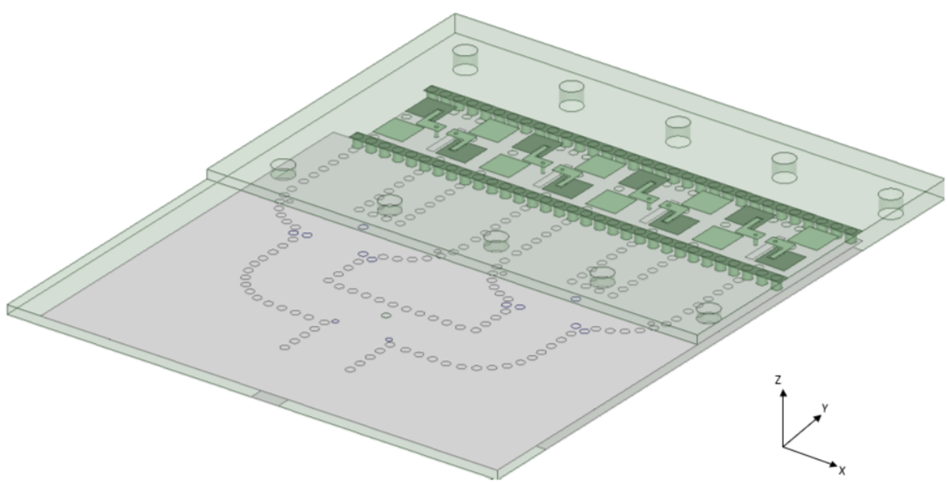

Figure 4.5: 3D view of the proposed linear array

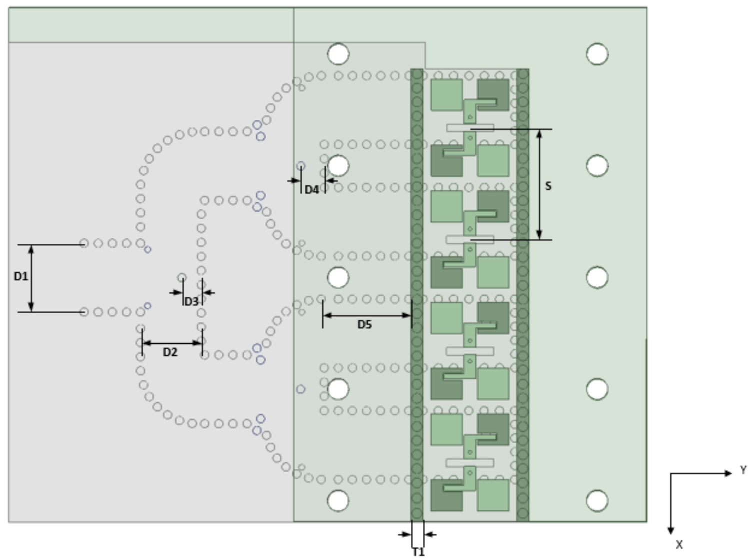

(a) Top view

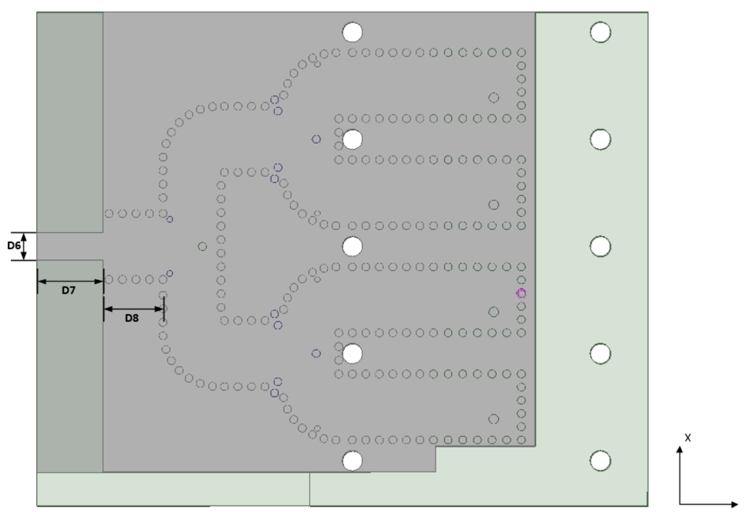

(b) Bottom View

Figure 4.6: Geometry of the proposed antenna array

4.4 Measurement and Discussion

To verify the proposed antenna array, the array is fabricated using the standard single-layer PCB and plate-through-hole technologies, as shown in the Figure 4.7. The fixing screws have been used to combine two layers together and the SMP connector is connected to the end of the microstrip line to feed the antenna array. The $|S_{11}|$ is measured using the Ceyear 3672D (10MHz to 50GHz), while other parameters are measured in the same far-field anechoic chamber as the antenna element prototype. The array setup is shown in the Figure 4.8. Due to the limitation of the measurement environment, only the upper hemisphere of the radiation pattern is considered.

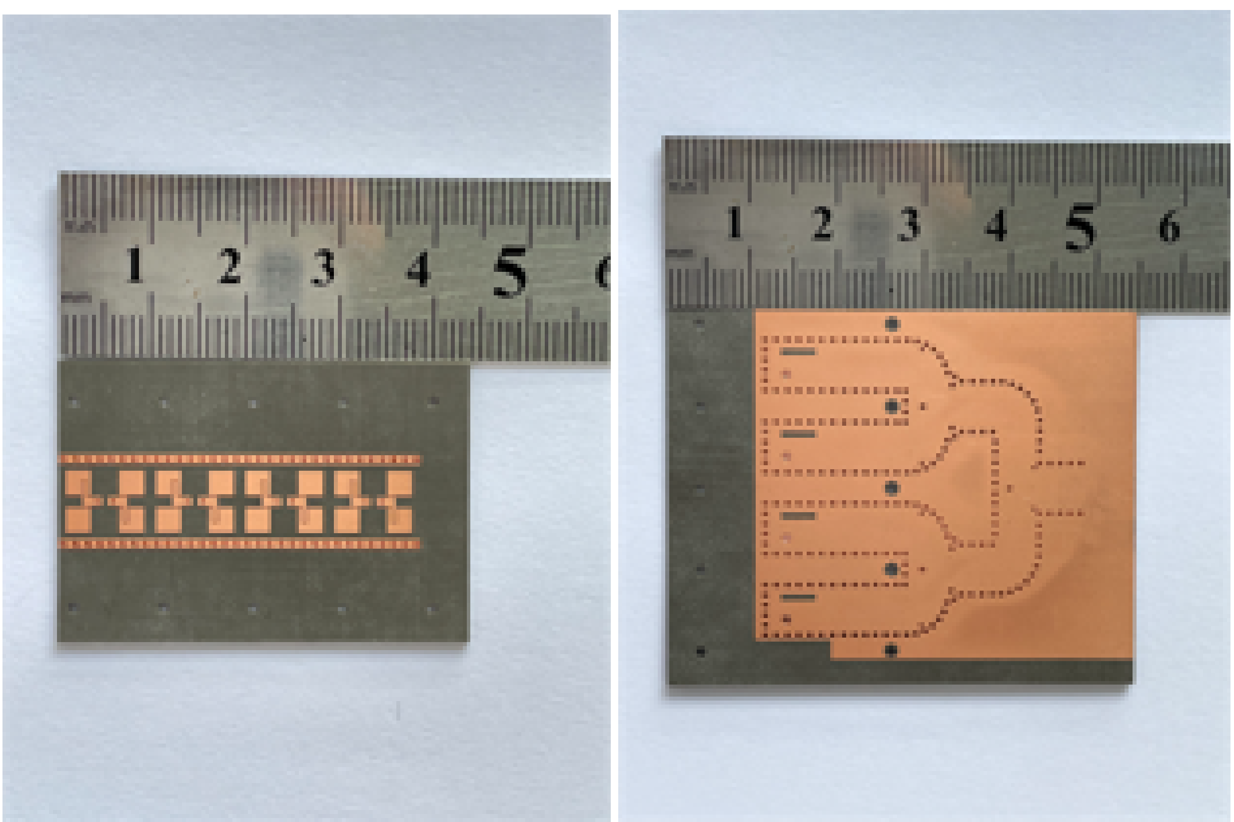

(a) Top layer **(b)** Bottom Layer

Figure 4.7: Fabricated antenna array before assembly

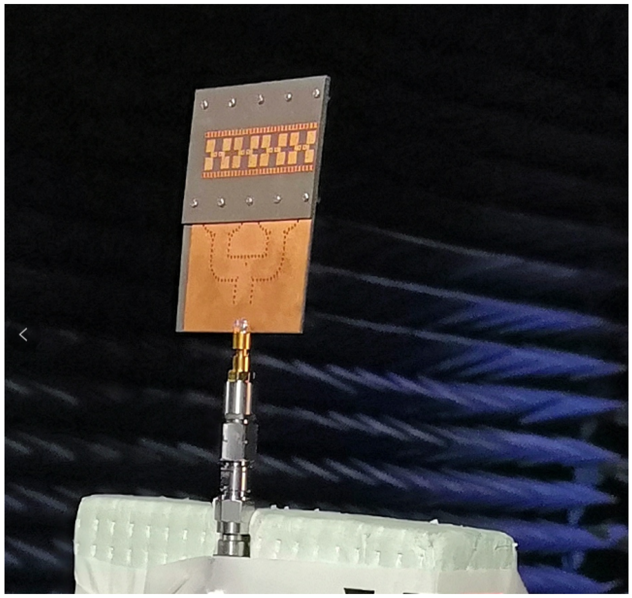

Figure 4.8: Assembled proposed antenna array in the anechoic chamber

The simulated and measured results are shown in the Figure 4.9 and 4.10. The simulated and measured impedance bandwidth are 15.40%(from 26.13 to 30.49 GHz) and 17.39% (from 25.42 to 30.26GHz), respectively. The simulated and measured 3dB AR bandwidth are 15.71%(from 25.99 to 30.42GHz) and 16.93%(from 25.57 to 30.30GHz). The fabricated array has reached a measured gain of 12 $\pm$ 0.9 dBic over the operating band. Moreover, a good agreement between simulated and measured radiation patterns has been achieved. The deviation between the simulated and measured results is mainly caused by the connector and fabrication error. One limitation of this antenna array is the slightly high sidelobe level (SLL). It is mainly due to the large spacing between elements. One way to reduce it is to utilize multi-layer structures. A comparison between the proposed antenna array with other mmWave antenna arrays using uniformly distributed networks is listed in the Table 4.2. With the help of the proposed low-profile wideband antenna element, the proposed array achieves a wide overlapped bandwidth of 16.8% and a height of only $0.2\lambda_s$.

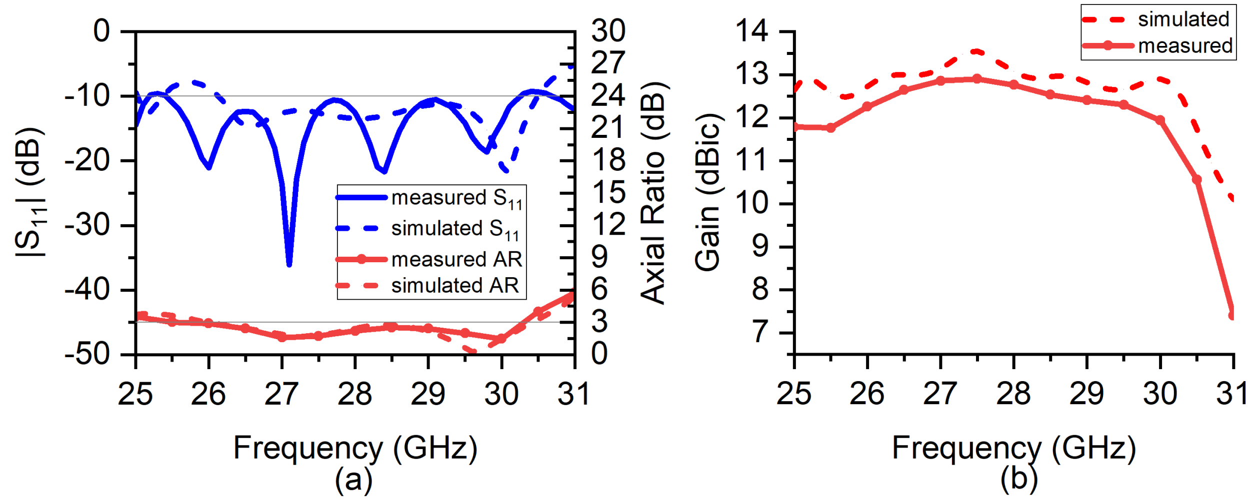

Figure 4.9: Simulated and measured (a) $|S_{11}|$, AR and (b) gain of the proposed antenna array

Table 4.2: Performance comparison between the proposed antenna array with other antenna arrays using uniformly netowkrs in the millimeter band

Ref.	Element Number	Feeding network	Element type	Overlap. BW	Peak gain(dBic)	Thickness(λ_s)
[49]	2x2	Microstrip lines	ME-dipole	11.33%	13.12	0.24
[28]	8x8	SIW	ME-dipole	16.39%	26.1	0.71
[45]	4x4	SIW	Slot with parasitic patch	14%	18.2	0.28
[27]	4x4	SIW	Aperture-coupled patch	10.6%	12.5	0.49
This work	1x4	SIW	ME-dipole with parasitic patch	16.8%	12.9	0.2

Overlap. BW is defined as the range of frequencies which have $|S_{11}| < -10dB$ and $AR < 3dB$

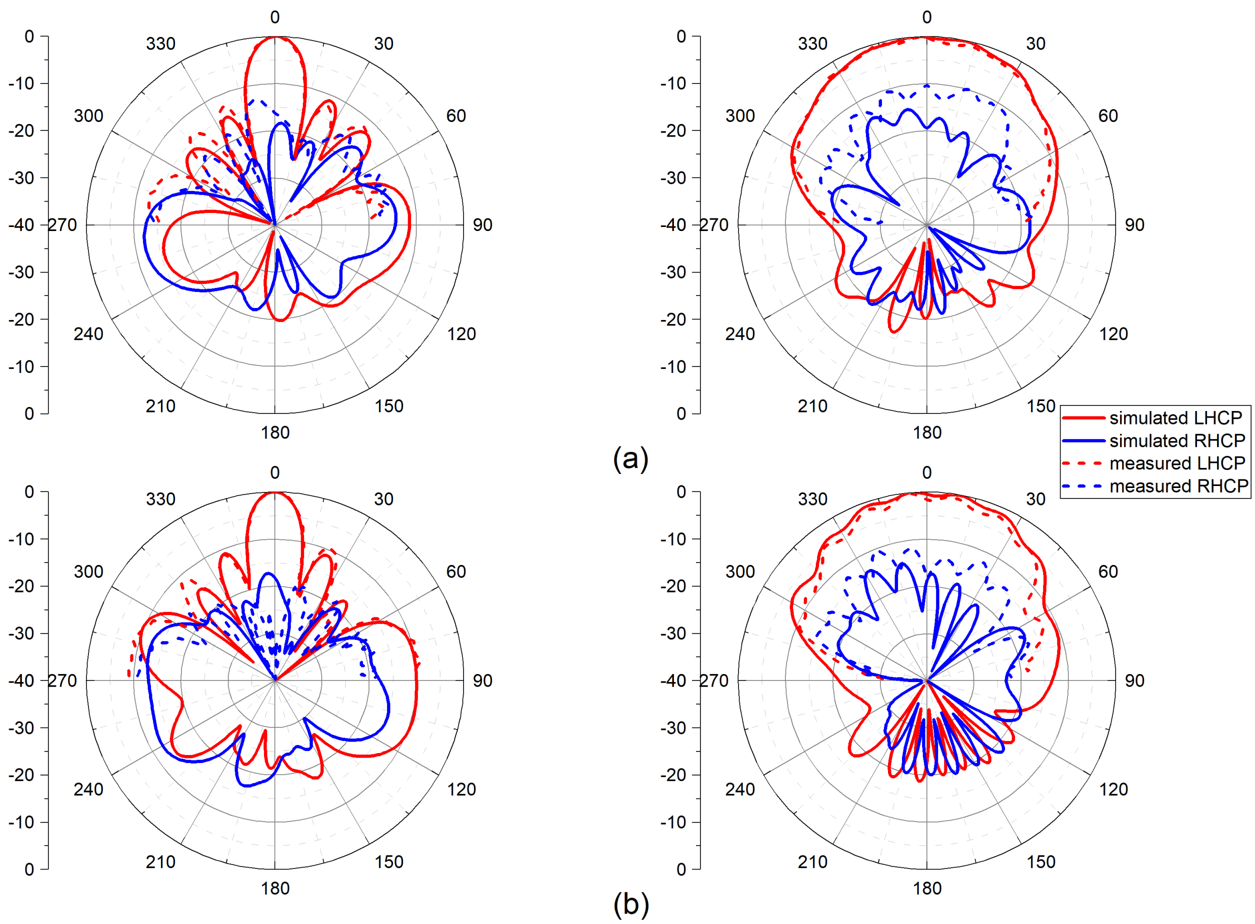

Figure 4.10: Simulated and measured radiation patterns of *XOZ* plane(left) and *YOZ* plane(right) of the proposed antenna array at (a)27GHz and (b)29GHz

Chapter 5

Conclusions

In this thesis, a low-profile wideband magnetic-electric dipole antenna with parasitic patches is proposed. The antenna element achieves a wide impedance and AR bandwidth of 22.1% (from 24.64 to 30.77GHz) and 20.1% (from 25.22 to 30.85GHz), respectively. To verify the performance of the antenna element, an antenna prototype that combines the antenna element with additional transmission lines and walls has been designed, fabricated, and measured. Due to the above changes, the prototype has different results; the fabricated antenna prototype has a measured impedance and 3dB-AR bandwidth of 19.7%(from 24.96 to 30.4GHz) and 17.5%(from 25.67 to 30.59GHz) respectively, and a gain of 7.2 $\pm$ 1.1 dBic over the operating band. Finally, a four-element linear circularly polarized antenna array with a SIW feeding network has been designed and fabricated. This antenna array has achieved a measured impedance and 3dB-AR bandwidth of 17.39%(from 25.42 to 30.26GHz) and 16.93%(from 25.57 to 30.30GHz) respectively with a peak gain of 12.9dBic without using the squential feed.

5.1 Future Work

Even though the proposed antenna element and array have achieved desired low-profile and wideband characteristics, certain drawbacks still require more future works to solve include:

1. The main cause of the high sidelobe level is the large spacing between elements. Some ways such as sequential rotated network and multidimensional network arrangement could be further investigated.

2. The extra ground plane and substrate could greatly impact the AR performance of antennas. In this thesis, two walls have been used to reduce such effects. However, it is worth implementing a whole cavity to further reduce the influence.

3. The proposed ME dipole antennas have only modified the electric dipole to generate CP radiation due to their simplicity while the magnetic dipole remains linear polarized similar to works [37] [21]. To further improve the antenna's performance, it is worth introducing the CP magnetic dipole component when the time and resources are available.

4. Even though the SIW has already achieved the lower transmission loss comparing to conventional transmission lines, it is still filled with dielectric materials due to the cost concerns. One way to reduce it is to utilize air-filled SIW [33], especially for arrays with larger dimensions.

Bibliography

[1] Abdel-Wahab, W. M., and Safavi-Naeini, S. Wide-bandwidth 60-ghz aperture-coupled microstrip patch antennas (mpas) fed by substrate integrated waveguide (siw). *IEEE Antennas and Wireless Propagation Letters 10* (2011), 1003–1005.

[2] Andrews, J. G., Buzzi, S., Choi, W., Hanly, S. V., Lozano, A., Soong, A. C. K., and Zhang, J. C. What will 5g be? *IEEE Journal on Selected Areas in Communications 32*, 6 (2014), 1065–1082.

[3] Ansys, Inc. *Ansys HFSS*, 2020 [Online]. `https://www.ansys.com/products/electronics/ansys-hfss`.

[4] Bai, X., Qu, S.-W., Yang, S., Hu, J., and Nie, Z.-P. Millimeter-wave circularly polarized tapered-elliptical cavity antenna with wide axial-ratio beamwidth. *IEEE Transactions on Antennas and Propagation 64*, 2 (2016), 811–814.

[5] Balanis, C. A. *Antenna theory: analysis and design*. Wiley, 2016.

[6] Bogale, T. E., Wang, X., and Le, L. *mmWave communication enabling techniques for 5G wireless systems*. 01 2017, pp. 195–225.

[7] CHANDRAPPA, D. K. Substrate integrated waveguide based millimeter wave antennas. Master's thesis, Concordia University, October 2019.

[8] CHLAVIN, A. A new antenna feed having equal e -and h-plane patterns. *Transactions of the IRE Professional Group on Antennas and Propagation 2*, 3 (1954), 113–119.

[9] COMMONS, W. File:waveguide17-with-ubr120-flanges.svg — wikimedia commons, the free media repository, 2020. [Online; accessed 13-August-2021].

[10] DESLANDES, D., AND WU, K. Integrated microstrip and rectangular waveguide in planar form. *IEEE Microwave and Wireless Components Letters 11*, 2 (2001), 68–70.

[11] DESLANDES, D., AND WU, K. Accurate modeling, wave mechanisms, and design considerations of a substrate integrated waveguide. *IEEE Transactions on Microwave Theory and Techniques 54*, 6 (2006), 2516–2526.

[12] FENG, B., LAI, J., CHUNG, K. L., CHEN, T.-Y., LIU, Y., AND SIM, C.-Y.-D. A compact wideband circularly polarized magneto-electric dipole antenna array for 5g millimeter-wave application. *IEEE Transactions on Antennas and Propagation 68*, 9 (2020), 6838–6843.

[13] GE, L., AND LUK, K. M. A low-profile magneto-electric dipole antenna. *IEEE Transactions on Antennas and Propagation 60*, 4 (2012), 1684–1689.

[14] GE, L., AND LUK, K. M. A magneto-electric dipole antenna with low-profile and simple structure. *IEEE Antennas and Wireless Propagation Letters 12* (2013), 140–142.

[15] Guan, D.-F., Ding, C., Qian, Z.-P., Zhang, Y.-S., Jay Guo, Y., and Gong, K. Broadband high-gain siw cavity-backed circular-polarized array antenna. *IEEE Transactions on Antennas and Propagation 64*, 4 (2016), 1493–1497.

[16] Guntupalli, A. B., and Wu, K. 60-ghz circularly polarized antenna array made in low-cost fabrication process. *IEEE Antennas and Wireless Propagation Letters 13* (2014), 864–867.

[17] Hirokawa, J. Plate-laminated waveguide slot array antennas and its polarization conversion layers. *Automatika 53* (04 2012).

[18] Hirokawa, J., and Ando, M. Single-layer feed waveguide consisting of posts for plane tem wave excitation in parallel plates. *IEEE Transactions on Antennas and Propagation 46*, 5 (1998), 625–630.

[19] Hong, W., Baek, K., Lee, Y., Kim, Y., and Ko, S. Study and prototyping of practically large-scale mmwave antenna systems for 5g cellular devices. *IEEE Communications Magazine 52*, 9 (2014), 63–69.

[20] Huang, J. A technique for an array to generate circular polarization with linearly polarized elements. *IEEE Transactions on Antennas and Propagation 34*, 9 (1986), 1113–1124.

[21] Kang, K., Shi, Y., and Liang, C.-H. A wideband circularly polarized magnetoelectric dipole antenna. *IEEE Antennas and Wireless Propagation Letters 16* (2017), 1647–1650.

[22] KILDAL, P. Three metamaterial-based gap waveguides between parallel metal plates for mm/submm waves. In *2009 3rd European Conference on Antennas and Propagation* (2009), pp. 28–32.

[23] KORDIBOROUJENI, Z., AND BORNEMANN, J. New wideband transition from microstrip line to substrate integrated waveguide. *IEEE Transactions on Microwave Theory and Techniques 62*, 12 (2014), 2983–2989.

[24] LAI, H. W., AND WONG, H. Substrate integrated magneto-electric dipole antenna for 5g wi-fi. *IEEE Transactions on Antennas and Propagation 63*, 2 (2015), 870–874.

[25] LI, L., CHEN, X., KHAZAKA, R., AND WU, K. A transition from substrate integrated waveguide (siw) to rectangular waveguide. In *2009 Asia Pacific Microwave Conference* (2009), pp. 2605–2608.

[26] LI, M., AND LUK, K.-M. A wideband circularly polarized antenna for microwave and millimeter-wave applications. *IEEE Transactions on Antennas and Propagation 62*, 4 (2014), 1872–1879.

[27] LI, Y., CHEN, Z. N., QING, X., ZHANG, Z., XU, J., AND FENG, Z. Axial ratio bandwidth enhancement of 60-ghz substrate integrated waveguide-fed circularly polarized ltcc antenna array. *IEEE Transactions on Antennas and Propagation 60*, 10 (2012), 4619–4626.

[28] LI, Y., AND LUK, K.-M. A 60-ghz wideband circularly polarized aperture-coupled magneto-electric dipole antenna array. *IEEE Transactions on Antennas and Propagation 64*, 4 (2016), 1325–1333.

[29] Luk, K.-M., and Wong, H. A new wideband unidirectional antenna element. *Int. J. Microw. Opt. Technol. 1*, 1 (2006), 35–44.

[30] Luk, K.-M., and Wu, B. The magnetoelectric dipole—a wideband antenna for base stations in mobile communications. *Proceedings of the IEEE 100*, 7 (2012), 2297–2307.

[31] Mazouni, K., Zeitler, A., Lanteri, J., Pichot, C., Dauvignac, J. ., Migliaccio, C., Yonemoto, N., Kohmura, A., and Futatsumori, S. 76.5 ghz millimeter-wave radar for foreign object debris detection on airport runways. In *2011 8th European Radar Conference* (2011), pp. 222–225.

[32] Miura, Y., Hirokawa, J., Ando, M., Igarashi, K., and Yoshida, G. A circularly-polarized aperture array antenna with a corporate-feed hollow-waveguide circuit in the 60 ghz-band. In *2011 IEEE International Symposium on Antennas and Propagation (APSURSI)* (2011), pp. 3029–3032.

[33] Parment, F., Ghiotto, A., Vuong, T.-P., Duchamp, J.-M., and Wu, K. Air-filled substrate integrated waveguide for low-loss and high power-handling millimeter-wave substrate integrated circuits. *IEEE Transactions on Microwave Theory and Techniques 63*, 4 (2015), 1228–1238.

[34] Rappaport, T. *Wireless Communications: Principles and Practice, 2nd Edition*, vol. 2. 12 2001.

[35] Ruan, X., Qu, S.-W., Zhu, Q., Ng, K. B., and Chan, C. H. A complementary circularly polarized antenna for 60-ghz applications. *IEEE Antennas and Wireless Propagation Letters 16* (2017), 1373–1376.

[36] SHAKEEB, M. Circularly polarized microstrip antenna. Master's thesis, Concordia University, 2011.

[37] SHI, Y., CAI, Y., ZHANG, X.-F., AND KANG, K. A simple tri-polarization reconfigurable magneto-electric dipole antenna. *IEEE Antennas and Wireless Propagation Letters 17*, 2 (2018), 291–294.

[38] STANLEY, M., HUANG, Y., LOH, T., XU, Q., WANG, H., AND ZHOU, H. A high gain steerable millimeter-wave antenna array for 5g smartphone applications. In *2017 11th European Conference on Antennas and Propagation (EUCAP)* (2017), pp. 1311–1314.

[39] STUTZMAN, W. L., AND THIELE, G. A. *Antenna theory and design*. Wiley, 2013.

[40] SUN, H., GUO, Y.-X., AND WANG, Z. 60-ghz circularly polarized u-slot patch antenna array on ltcc. *IEEE Transactions on Antennas and Propagation 61*, 1 (2013), 430–435.

[41] TARINGOU, F., AND BORNEMANN, J. New substrate-integrated to coplanar waveguide transition. In *2011 41st European Microwave Conference* (2011), pp. 428–431.

[42] WANG, M., ZHU, Q., AND CHAN, C. H. Wideband, low-profile slot-fed dipole-patch antenna and array. *IEEE Antennas and Wireless Propagation Letters 19*, 12 (2020), 2250–2254.

[43] WANG, Y.-F., WU, B., ZHANG, N., ZHAO, Y.-T., AND SU, T. Wideband circularly polarized magneto-electric dipole 1×2 antenna array for millimeter-wave applications. *IEEE Access 8* (2020), 27516–27523.

[44] WILKINSON, E. An n-way hybrid power divider. *IRE Transactions on Microwave Theory and Techniques 8*, 1 (1960), 116–118.

[45] WU, J., CHENG, Y. J., AND FAN, Y. Millimeter-wave wideband high-efficiency circularly polarized planar array antenna. *IEEE Transactions on Antennas and Propagation 64*, 2 (2016), 535–542.

[46] XU, F., AND WU, K. Guided-wave and leakage characteristics of substrate integrated waveguide. *IEEE Transactions on Microwave Theory and Techniques 53*, 1 (2005), 66–73.

[47] XU, H., ZHOU, J., ZHOU, K., WU, Q., YU, Z., AND HONG, W. Planar wideband circularly polarized cavity-backed stacked patch antenna array for millimeter-wave applications. *IEEE Transactions on Antennas and Propagation 66*, 10 (2018), 5170–5179.

[48] XU, J., HONG, W., JIANG, Z. H., CHEN, J., AND ZHANG, H. A q-band low-profile dual circularly polarized array antenna incorporating linearly polarized substrate integrated waveguide-fed patch subarrays. *IEEE Transactions on Antennas and Propagation 65*, 10 (2017), 5200–5210.

[49] XU, J., HONG, W., JIANG, Z. H., AND ZHANG, H. Low-cost millimeter-wave circularly polarized planar integrated magneto-electric dipole and its arrays with low-profile feeding structures. *IEEE Antennas and Wireless Propagation Letters 19*, 8 (2020), 1400–1404.

[50] XU, J., HONG, W., JIANG, Z. H., AND ZHANG, H. Millimeter-wave broadband substrate integrated magneto-electric dipole arrays with corporate low-profile mi-

crostrip feeding structures. *IEEE Transactions on Antennas and Propagation 68*, 10 (2020), 7056–7067.

[51] YANG, S., LEE, K.-F., KISHK, A., AND LUK, K. Design and study of wide band single feed circularly polarized microstrip antenna. *Progress In Electromagnetics Research 80* (01 2008), 45–61.

[52] YANG, Z., PATHAK, P. H., ZENG, Y., LIRAN, X., AND MOHAPATRA, P. Monitoring vital signs using millimeter wave. In *Proceedings of the 17th ACM International Symposium on Mobile Ad Hoc Networking and Computing* (New York, NY, USA, 2016), MobiHoc '16, Association for Computing Machinery, p. 211–220.

[53] ZHU, C., XU, G., DING, D., WU, J., WANG, W., HUANG, Z., AND WU, X. Low profile wideband millimeter wave circularly polarized antenna with hexagonal parasitic patches. *IEEE Antennas and Wireless Propagation Letters* (2021), 1–1.

[54] ZHU, Q. *Design of millimeter-wave substrate integrated waveguide antennas and arrays for 5G applications*. PhD thesis, 2018.